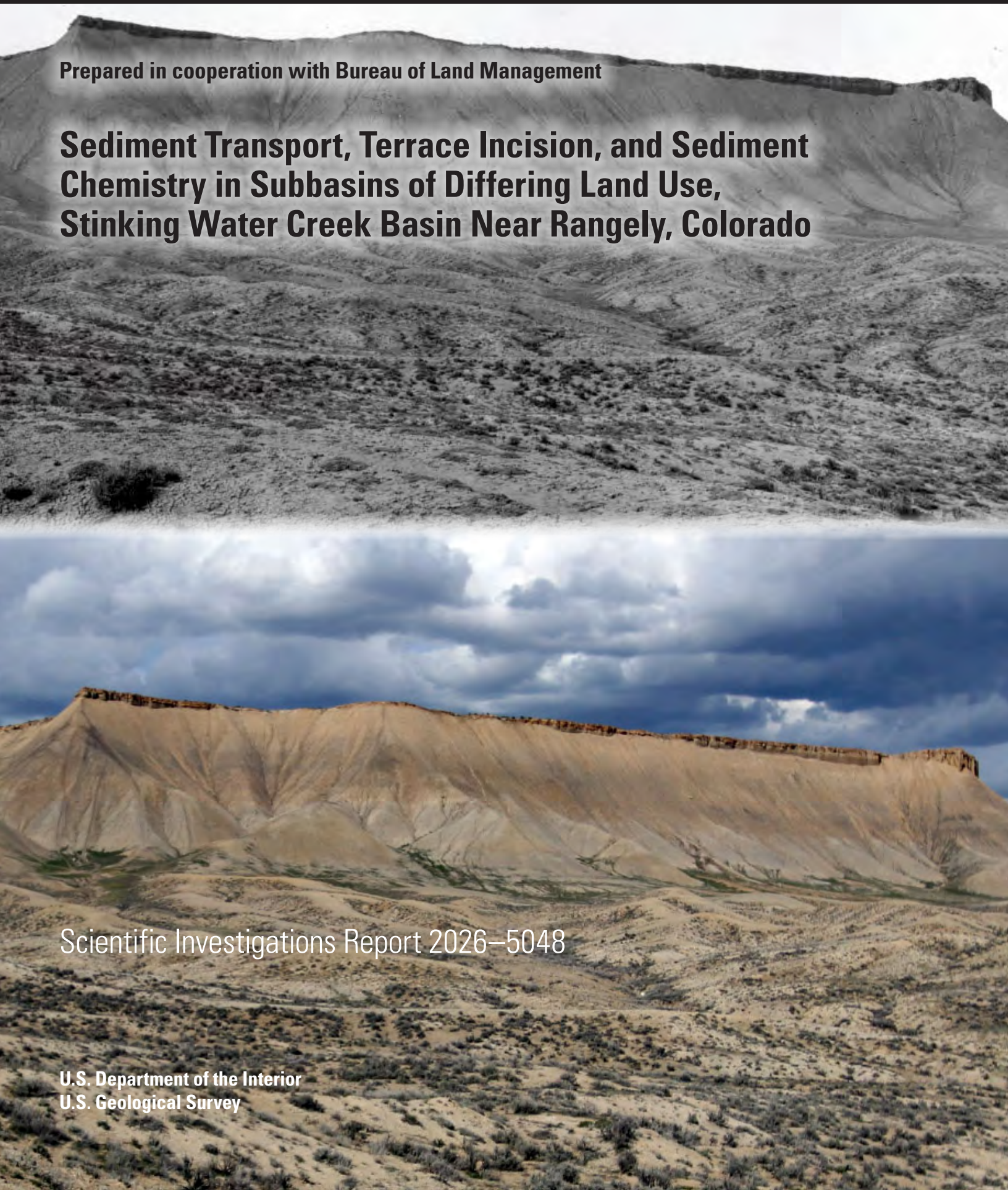
USGS
science for a changing world

Prepared in cooperation with Bureau of Land Management

Sediment Transport, Terrace Incision, and Sediment Chemistry in Subbasins of Differing Land Use, Stinking Water Creek Basin Near Rangely, Colorado



Scientific Investigations Report 2026–5048

U.S. Department of the Interior
U.S. Geological Survey

Cover. Photographs (fig. 9 of this report) of landscape near Stinking Water Creek, near Rangely, Colorado, in 1907 (from Gale, 1908) and 2019 (photograph by Cory A. Williams, U.S. Geological Survey).

Sediment Transport, Terrace Incision, and Sediment Chemistry in Subbasins of Differing Land Use, Stinking Water Creek Basin Near Rangely, Colorado

By Rachel G. Gidley, Shannon A. Mahan, Emma T. Krolczyk, Cory A. Williams, Michael S. Kohn, Michael R. Stevens, and Joel W. Homan

Prepared in cooperation with Bureau of Land Management

Scientific Investigations Report 2026–5048

U.S. Department of the Interior
U.S. Geological Survey

U.S. Geological Survey, Reston, Virginia: 2026

For more information on the USGS—the Federal source for science about the Earth, its natural and living resources, natural hazards, and the environment—visit https://www.usgs.gov.

For an overview of USGS information products, including maps, imagery, and publications, visit https://store.usgs.gov/ or contact the store at 1–888–275–8747.

Any use of trade, firm, or product names is for descriptive purposes only and does not imply endorsement by the U.S. Government.

Although this information product, for the most part, is in the public domain, it also may contain copyrighted materials as noted in the text. Permission to reproduce copyrighted items must be secured from the copyright owner.

Suggested citation:
Gidley, R.G., Mahan, S.A., Krolczyk, E.T., Williams, C.A., Kohn, M.S., Stevens, M.R., and Homan, J.W., 2026, Sediment transport, terrace incision, and sediment chemistry in subbasins of differing land use, Stinking Water Creek Basin near Rangely, Colorado: U.S. Geological Survey Scientific Investigations Report 2026–5048, 38 p., https://doi.org/10.3133/sir20265048.

Associated data for this publication:
Gidley, R.G., Williams, C.A., Stevens, M.R., Kohn, M.S., and Homan, J.W., 2026, Landscape alteration, sediment chemistry, cross section, sediment transport, and load data for Stinking Water Creek, Rio Blanco County, Colorado, 2015–20: U.S. Geological Survey data release, https://doi.org/10.5066/P9R3YPO1.

Mahan, S.A., Krolczyk, E.T., and Gidley, R.G., 2026, Geochronologic data for selected subbasins of Stinking Water Gulch, Rio Blanco County, Colorado, 2015–2020: U.S. Geological Survey data release, https://doi.org/10.5066/P9KLLFQT.

Preston, T.M., Day, N.K., Adams, J.D., and Holmquist-Johnson, C.L., 2021, Orthoimagery, digital elevation, digital terrain, final surface, and vegetation classification models for four stream catchments in western Colorado 2016: U.S. Geological Survey data release, https://doi.org/10.5066/P91KRAAD.

ISSN 2328-0328 (online)

Contents

Abstract....1
Plain Language Summary....1
Introduction....1
Purpose and Scope....2
Study Area Description....4
History of Energy Development....4
History of Rangeland Grazing....4
Arroyo System Geomorphology and History....7
Methods....8
Historical Aerial Photographs....8
Real-Time Kinematic Global Navigation Satellite Systems Survey and Uncrewed Aerial Systems Survey....8
Channel Morphology....9
Sediment Chemistry, Dating, and Density....9
Sediment Chemistry....9
Optically Stimulated Luminescence Dating....11
Sediment Density....12
Sediment Transport Models....12
Incision Rates and Load Estimates....12
Results....13
Timeline of Land-Use Change....13
Channel Morphology....13
Sediment Density and Chemistry....13
Luminescence Dating....16
Sediment Transport Models....16
Incision Rates and Load Estimates....19
Discussion....20
Timelines and Effects of Land Use on Channel Morphology....20
Luminescence Ages and Channel History....25
Sediment Density and Chemistry....26
Sediment, Salinity, and Selenium Loads....27
Potential Additional Geochronology Studies....27
Summary....29
References Cited....30

Figures

1. Map showing location of the Rangely Oil Field, Stinking Water Creek Basin, and lower White River Basin, western Colorado....3
2. Locations of four selected subbasins of Stinking Water Creek, near Rangely, Colorado....5
3. Roads and oil well pad locations in Stinking Water Creek Basin near Rangely, Colorado....6

4. Stinking Water Creek subbasin A1 sampling location photograph and cross-section profile....10
5. Percentage of disturbed area in four selected subbasins of Stinking Water Creek near Rangely, Colorado, 1882–2013....14
6. Disturbance types observed in 2013 aerial photographs of four selected subbasins of Stinking Water Creek Basin near Rangely, Colorado....14
7. Summary of upper terrace to streambed cross-section area, depth, width, and width-to-depth ratio in the four subbasins....22
8. Summary of lower terrace to streambed cross-section area, depth, width, and width-to-depth ratio in the four subbasins....23
9. Photographs of landscape near Stinking Water Creek, near Rangely, Colorado, in 1907 and 2019....24
10. Potential channel history determined from optically stimulated luminescence dating in four subbasins, which are local terraces to the main stem of Stinking Water Creek, near Rangely, Colorado....28

Tables

1. Comparison of channel morphology characteristics for 0.10 annual exceedance probability streamflow determined for 48 ephemeral streams in the Grand Valley, western Colorado, near Rangely, Colorado....14
2. Bulk density of sediment samples collected on the main stem of Stinking Water Creek, near Rangely, Colorado....15
3. Total dissolved solids concentrations of sediment samples from selected subbasins of Stinking Water Creek near Rangely, Colorado....15
4. Sequential selenium extraction concentrations of sediment samples from selected subbasins of Stinking Water Creek near Rangely, Colorado....16
5. Optically stimulated luminescence quartz results for sediment samples from selected subbasins of Stinking Water Creek near Rangely, Colorado....17
6. Water Erosion Prediction Project model results for Stinking Water Creek subbasins near Rangely, Colorado....18
7. Water Erosion Prediction Project road input parameters and model results for Stinking Water Creek subbasins near Rangely, Colorado....18
8. Estimated incision rates, change in channel volume, and associated sediment, salinity, and selenium mass results for Stinking Water Creek subbasins near Rangely, Colorado....19
9. Estimated sediment, salinity, and selenium annual load results for Stinking Water Creek subbasins near Rangely, Colorado....19
10. Selected subbasin properties and results for Stinking Water Creek subbasins near Rangely, Colorado....20

Conversion Factors

International System of Units to U.S. customary units

Multiply	By	To obtain
	Length	
centimeter (cm)	0.3937	inch (in.)
millimeter (mm)	0.03937	inch (in.)
meter (m)	3.281	foot (ft)
kilometer (km)	0.6214	mile (mi)
	Area	
hectare (ha)	2.471	acre
square kilometer (km^2)	247.1	acre
hectare (ha)	0.003861	square mile (mi^2)
square kilometer (km^2)	0.3861	square mile (mi^2)
	Volume	
liter (L)	0.2642	gallon (gal)
	Flow rate	
cubic meter per year (m^3/yr)	0.000811	acre-foot per year (acre-ft/yr)
	Mass	
gram (g)	0.03527	ounce, avoirdupois (oz)
kilogram (kg)	2.205	pound avoirdupois (lb)
kilogram per year (kg/yr)	2.295	pound per year (lb/yr)
metric ton (t)	1.102	ton, short [2,000 lb]
metric ton (t)	0.9842	ton, long [2,240 lb]
ton per year (t/yr)	1.102	ton, short [2,000 lb] per year
ton per year (t/yr)	0.9842	ton, long [2,240 lb] per year
	Density	
gram per cubic centimeter (g/cm^3)	62.4220	pound per cubic foot (lb/ft^3)

Temperature in degrees Celsius (°C) may be converted to degrees Fahrenheit (°F) as follows:

$$°F = (1.8 \times °C) + 32.$$

Datums

Vertical coordinate information is referenced to the North American Vertical Datum of 1988 (NAVD 88).

Horizontal coordinate information is referenced to the North American Datum of 1983 (NAD 83).

Elevation, as used in this report, refers to distance above the vertical datum.

Supplemental Information

Concentrations of chemical constituents in water are in milligrams per liter (mg/L). Concentrations of chemical constituents in sediment are given either in milligrams per kilogram of dry sediment (mg/kg) or micrograms per gram of dry sediment (µg/g).

Results for optically stimulated luminescence dating are commonly expressed as the units of absorbed radiation in Gray (Gy) per time. The standard international format for units is Gray/ka, where ka = thousands of years, or Gy/yr, where yr = one calendar year.

Abbreviations

DEM	digital elevation model
D_R	dose rate
DTM	digital terrain model
GNSS	Global Navigation Satellite System
GPS	Global Positioning System
NAD 83	North American Datum of 1983
NaOH	sodium hydroxide
Na_2SO_3	sodium sulfite
NAVD 88	North American Vertical Datum
OSL	optically stimulated luminescence
PRISM	Parameter-elevation Regressions on Independent Slopes Model
Q_{10}	0.10 annual exceedance probability streamflow
Qal	Quaternary alluvium
Qt1	Quaternary terrace 1
Qt2	Quaternary terrace 2
Qt3	Quaternary terrace 3
RTK	real-time kinematic
SSURGO	Soil Survey Geographic Database
TOPAZ	Topographic Parameterization program
TDS	total dissolved solids
UAS	uncrewed aerial system
USGS	U.S. Geological Survey
WEPP	Water Erosion Prediction Project

Sediment Transport, Terrace Incision, and Sediment Chemistry in Subbasins of Differing Land Use, Stinking Water Creek Basin Near Rangely, Colorado

By Rachel G. Gidley, Shannon A. Mahan, Emma T. Krolczyk, Cory A. Williams, Michael S. Kohn, Michael R. Stevens, and Joel W. Homan

Abstract

In many areas of western Colorado, Late Cretaceous Mancos Shale is a source of sediment, salinity, and selenium to surface water. Natural weathering processes and human activity can expose and move sediments from the Mancos Shale, leading to increased salinity and selenium concentrations in surface water. The U.S. Geological Survey, in cooperation with the Bureau of Land Management, studied four subbasins of Stinking Water Creek near Rangely, Colorado, to provide information regarding landscapes on Mancos Shale that have undergone land-use change. Rangeland grazing is present in all four subbasins. Subbasins A1 and A2 have land use related to energy development and subbasins B1 and B2 do not. Aerial photographs, sediment chemistry, optically stimulated luminescence (OSL) ages, cross-section surveys, and Watershed Erosion Prediction Project (WEPP) modeling were used to characterize the history of land-use change by estimating stream channel incision rates and sediment, salinity, and selenium loads.

All subbasins had upper and lower terraces and a modern streambed channel, and these surfaces were dated using OSL. In subbasins A1, A2, and B1, the streambed age was older than the terraces, indicating the channels are incising and widening into the older alluvium. In subbasin B2, however, the streambed age was much younger than the terraces, indicating aggradation is the main process.

Differences in channel morphology were not always related to land use but to the subbasin position (upstream compared to downstream). Channels in subbasins A1 and A2 were generally wider and shallower than channels in subbasins B1 and B2. Landscape disturbances related to energy development in subbasins A1 and A2 could have caused channel evolution to progress from incision to widening processes.

Plain Language Summary

Natural weathering processes and human activity disturbances on the Late Cretaceous Mancos Shale can release sediment, salinity, and selenium to surface water. Stinking Water Creek is an arroyo in western Colorado in an area that has experienced land-use change from rangeland grazing and oil and gas development. This report discusses optically stimulated luminescence dates and channel morphology data used to describe the geomorphic history of Stinking Water Creek. Understanding if and how land-use change affects channel storage and delivery of sediment, salinity, and selenium has important implications for management decisions in landscapes on Mancos Shale.

Introduction

In many areas of western Colorado, Late Cretaceous Mancos Shale is a major source of sediment, salinity, and selenium to surface waters (Butler and others, 1994; Presser and others, 1994; Elliott and others, 2008). Mancos Shale is about 1,052–1,265 meters (m) thick where exposed in the southern part of the Piceance and Uinta basins of Colorado and Utah and about 1,646 m thick in the central part of the Uinta basin (Hettinger and Kirschbaum, 2003). Seawater, volcanic ash, and pyrite are the primary sources of selenium to the Mancos Shale (Kulp and Pratt, 2004; Tuttle and others, 2014). Oxidation of pyrite formed selenium-bearing salts that have accumulated in the weathered zone for thousands of years (Tuttle and others, 2014) and are the most soluble forms of selenium in naturally weathered Mancos Shale and its derived materials (Mast and others, 2014). Natural weathering processes and human activity disturbances such as grazing, off highway vehicles, and road construction can expose and move sediments rich with selenium and salts, leading to increased concentrations of those constituents in streams and rivers (Tuttle and Grauch, 2009; Bern and others, 2015; Bern and others, 2023).

Scientific investigations have linked geologic sources and landscape disturbances to elevated concentrations of sediment, salinity, and selenium in waterways draining landscapes on Mancos Shale (Presser and others, 1994; Butler and others, 1996; Elliott and others, 2008). Human activity disturbances are the dominant processes affecting the distribution and storage of sediment, salinity, and selenium in and around channel areas, to varying degrees, due to changes in water delivery to and within the stream system and other basin processes (Butler and others, 1991, 1996; Hamilton, 1998; Bureau of Reclamation, 2005; Lemly, 2002; Hawkins and others, 2016; Bern and others, 2023). Understanding when and how some common land uses affect channel storage and delivery of these constituents can have important implications for management decisions.

Salinity and selenium are water-quality constituents of concern in areas with Mancos Shale (Tuttle and others, 2014). High salinity concentrations can damage agricultural crops and reduce yields as well as cause damage to pipes and water fixtures (Bureau of Reclamation, 2019). Selenium accumulates in the aquatic food chain, resulting in invertebrate mortality (deBruyn and Chapman, 2007; Conley and others, 2013; Henry and Wesner, 2018) as well as decreased reproduction, deformities, and mortality in fish and birds (Lemly, 1985; Ohlendorf and others, 1986; Ohlendorf, 1989; Presser, 1994; Chapman and others, 2010).

Efforts focused on reducing salinity in the Colorado River led to the creation of the Colorado River Basin Salinity Control Forum in 1973 to coordinate salinity control work among the Colorado River Basin States. The Colorado River Basin Salinity Control Act of 1974 authorized the Colorado River Basin Salinity Control Program, which focused on improving the Colorado River water quality (Colorado River Basin Salinity Control Forum, 2017). The Gunnison River Basin Selenium Management Program formed in response to a Programmatic Biological Opinion issued by the U.S. Fish and Wildlife Service (U.S. Fish and Wildlife Service, 2009), which stated the recovery of native Colorado fish species was hampered by selenium concentrations exceeding aquatic-life standards in the Gunnison River. These two basin-wide efforts allow resource managers and scientists to continue to understand and reduce salinity and selenium loads and sources in the Colorado River Basin, particularly in landscapes on Mancos Shale (Butler, 1996, 2001; Leib and others, 2012; Linard, 2013; Richards and Moore, 2015; Miller and others, 2017; McGwire and others, 2020; Bern and others, 2023; Williams and others, 2023).

A U.S. Geological Survey (USGS) assessment of undiscovered natural gas resources indicated the presence of substantial gas resources in the Mancos Shale within the Unita-Piceance Province (Hawkins and others, 2016; fig. 1). Exploration and development of natural gas resources from landscapes on Mancos Shale could lead to changes in water-quality conditions (for example, Bern and others, 2015); however, the long-term compared to short-term effects of potential future energy development on water-quality conditions in the region are unknown. Surface disturbances from expansion of road networks, oil and gas well pads, and oil and gas pipelines can increase vegetative disturbances and promote sediment transport during infrequent but intense precipitation. Surface alterations (soil compaction, vegetation denuding, road construction, and channel rerouting) and channel degradation (streambed incision and widening) along with increased rainfall runoff promote sediment, salinity, and selenium transport. Surface disturbances from energy infrastructure have similar potential to alter water quality, streamflow, channel morphology, and erosion rates in the area (Presser and others, 1994; Elliott and others, 2008; Belnap and others, 2009; Bern and others, 2015; Hawkins and others, 2016).

Beginning in 2015, the USGS, in cooperation with the Bureau of Land Management, studied four subbasins of Stinking Water Creek located within the lower White River Basin near Rangely, Colorado (fig. 2). The four subbasins are geographically similar but represent varied land-use histories of landscapes on Mancos Shale. The subbasins have exposed fluvial terraces for at least two incision events. Complicated land-use histories and the lack of historical water-quality and streamflow data necessitate an approach to estimate historical conditions and potential future effects of energy development on terraces formation, incision rates, and landscapes on Mancos Shale.

Purpose and Scope

The main purposes of this report are to: (1) provide information regarding landscapes on Mancos Shale with land-use change from rangeland grazing to energy development; (2) summarize land-use change and disturbances compiled from historical accounts and aerial photography; (3) provide a characterization of the transport of sediment, salinity, and selenium of four subbasins of Stinking Water Creek; (4) evaluate the role of land use on basin processes that may affect sediment, salinity, or selenium transport; (5) describe incision rates and sediment, salinity, and selenium loads estimated on the basis of channel morphology, optically stimulated luminescence (OSL) ages on terrace sediment, and Watershed Erosion Prediction Project (WEPP) hillslope (Flanagan and Nearing, 1995; Flanagan and others, 2013) and WEPP:Road (Elliott, 2021) sediment transport modeling; and (6) aid resource management decisions in areas of similar setting that could be affected by current (2026) and potential future energy development.

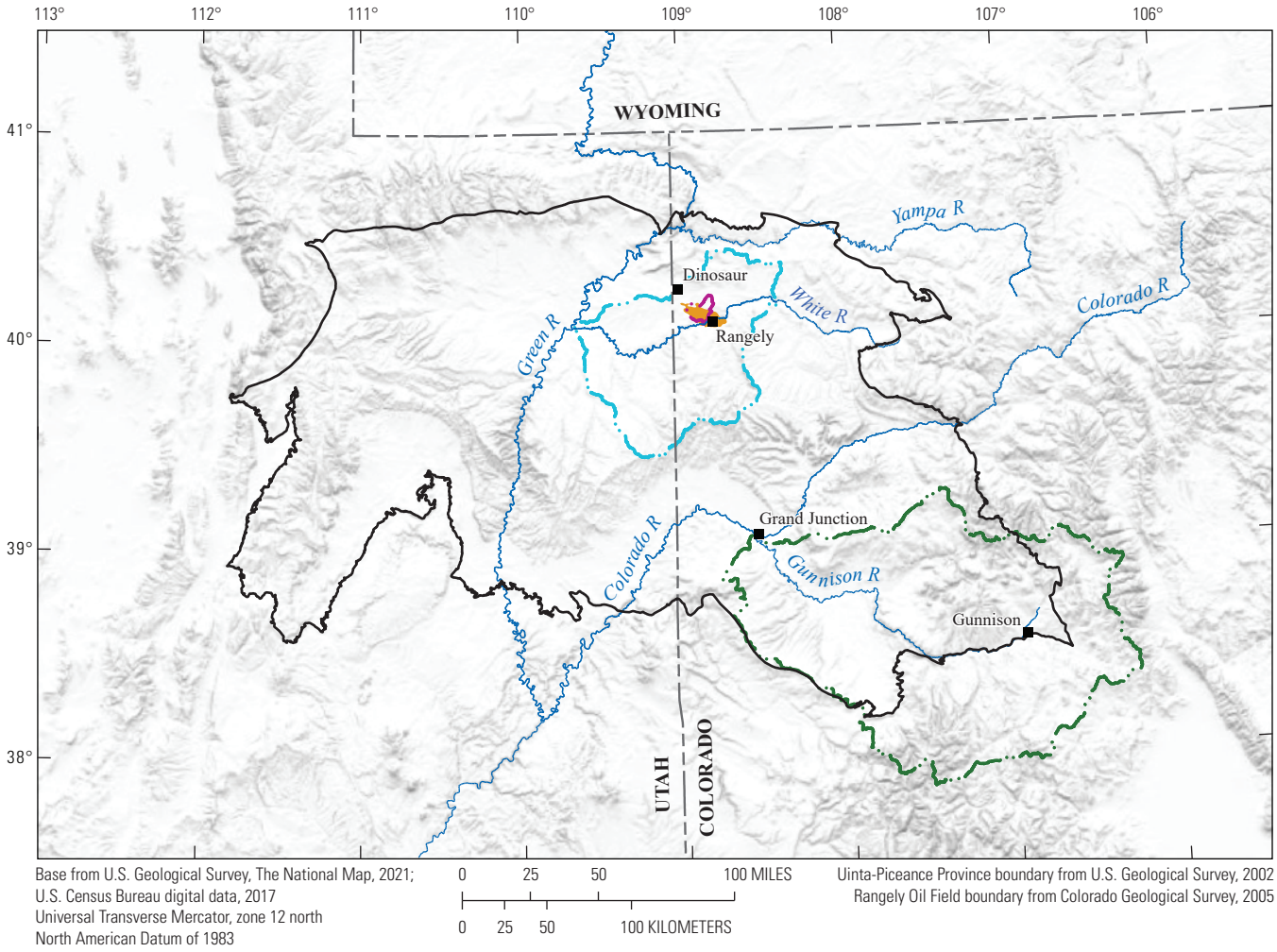


Figure 1. Map showing location of the Rangely Oil Field, Stinking Water Creek Basin, lower White River Basin, and Uinta-Piceance Province, western Colorado.

Study Area Description

The Stinking Water Creek Basin (112 square kilometers [km^2]) is in the lower White River Basin near Rangely, Colorado (U.S. Geological Survey, 2019). Public land in the area is used for rangeland grazing, energy (oil and gas) development, and recreation. Four subbasins underlain by Mancos Shale were selected for investigation (fig. 2): energy development is present in subbasins A1 (1.57 km^2) and A2 (1.41 km^2) but not in subbasins B1 (1.34 km^2) and B2 (1.63 km^2; U.S. Geological Survey, 2019; Villarreal and others, 2023; fig. 3). Rangeland grazing is present in all four subbasins (Luke McCarty, Bureau of Land Management, written commun., 2022). Subbasins A1 and B1 are adjacent to or near the main stem of Stinking Water Creek; subbasins A2 and B2 are further upstream (fig. 2). These subbasins were selected to allow for analysis of basin pairs with similar size, slope, and geology but different land use.

The study area is characterized by a semiarid climate (Beck and others, 2018). Mean annual precipitation in Rangely, Colorado, is 10.9 inches per year (1991–2020), and mean annual snowfall is 29.5 inches per year (National Centers for Environmental Information, 2023). The Stinking Water Creek Basin is bordered by rim rock, producing an escarpment rim below which are steep shale slopes and badlands. The land surface is hard, dry, and covered by sparse vegetation and biological soil crusts (Day and others, 2024). An early description in August 1907 (Gale, 1908, p. 9–16) characterized the area as,

> …"[a] desolate waste of dry washes and almost barren clay ridges, except only the immediate valley bottoms of White River. …Surface water runs off rapidly, cutting abrupt vertical-sided channels or miniature canyons even to a depth of 50 feet or more. These gullies rapidly extend and deepen with each succeeding flood, and in places the dissection becomes so intricate as to produce a typical badland. Areas of such topography, which characterizes much of Raven Park, are accessible only with much difficulty, and then only by avoiding the stream courses as far as possible and following the dividing ridges. ….[Stinking Water Gulch], like most of the other drainage channels of the region, is dry most of the summer except immediately after heavy showers, when it rims full with thick, muddy water for a few hours only. All these waters are heavily charged with alkaline salts."

History of Energy Development

The Rangely Oil Field near Rangely, Colorado (fig. 1) is one of the oldest and largest oil fields in the Rocky Mountain region. The Rangely Oil Field exploration began in the early 1870s and was documented during the Hayden Survey, which identified the area as Raven Park (Hayden, 1878). The original documentation of the area during the Hayden Survey suggested highly favorable conditions for large oil and gas resources within the Dakota Sandstone, believed to be at shallow depths below the Mancos Shale in the valley (Gale, 1908). Oil explorations began in 1901 among anticipation of artesian pressures and structural oil traps in the Dakota Sandstone, but they were largely unsuccessful. The wells from these explorations produced small amounts of oil and represented only a dozen or so attempts by 1907. Due to the remote nature of the area and low demand for oil, even the most productive well completed in the Weber Sandstone was capped and production was halted by 1933 (Colorado School of Mines, 2005).

Expansion of oil well drilling began in 1943 when World War II increased demand for oil. The Rangely Oil Field drilling increased with 182 wells in place by the end of 1945, and 478 wells drilled on 40-acre spacing by 1949. Falling pressure levels in the Rangely Oil Field led to the implementation of water-flooding operations in 1958 to increase production, and tertiary recovery using the carbon dioxide injection in conjunction with a supply pipeline that began in 1984. In 2005, there were 373 active producing wells, and 247 injection wells in the Rangely Oil Field (Colorado School of Mines, 2005).

History of Rangeland Grazing

Early reports of conditions in the Rangely Oil Field describe an area without consistent water sources available for livestock excluding the area adjacent to the White River (Gale, 1908). In 1882, herds of cattle were brought in and occupied areas along the Douglas Creek confluence with the White River (fig. 2). Cattle and sheep grazing increased in the area; however, owing to water limitations, grazing conditions along Stinking Water Creek were only conducive during winter months, when snow accumulation on the ground was sufficient to support water needs (Gale, 1908). More recent grazing allotments in the area were for sheep and generally were from late November through early April (Luke McCarty, Bureau of Land Management, written commun., 2022).

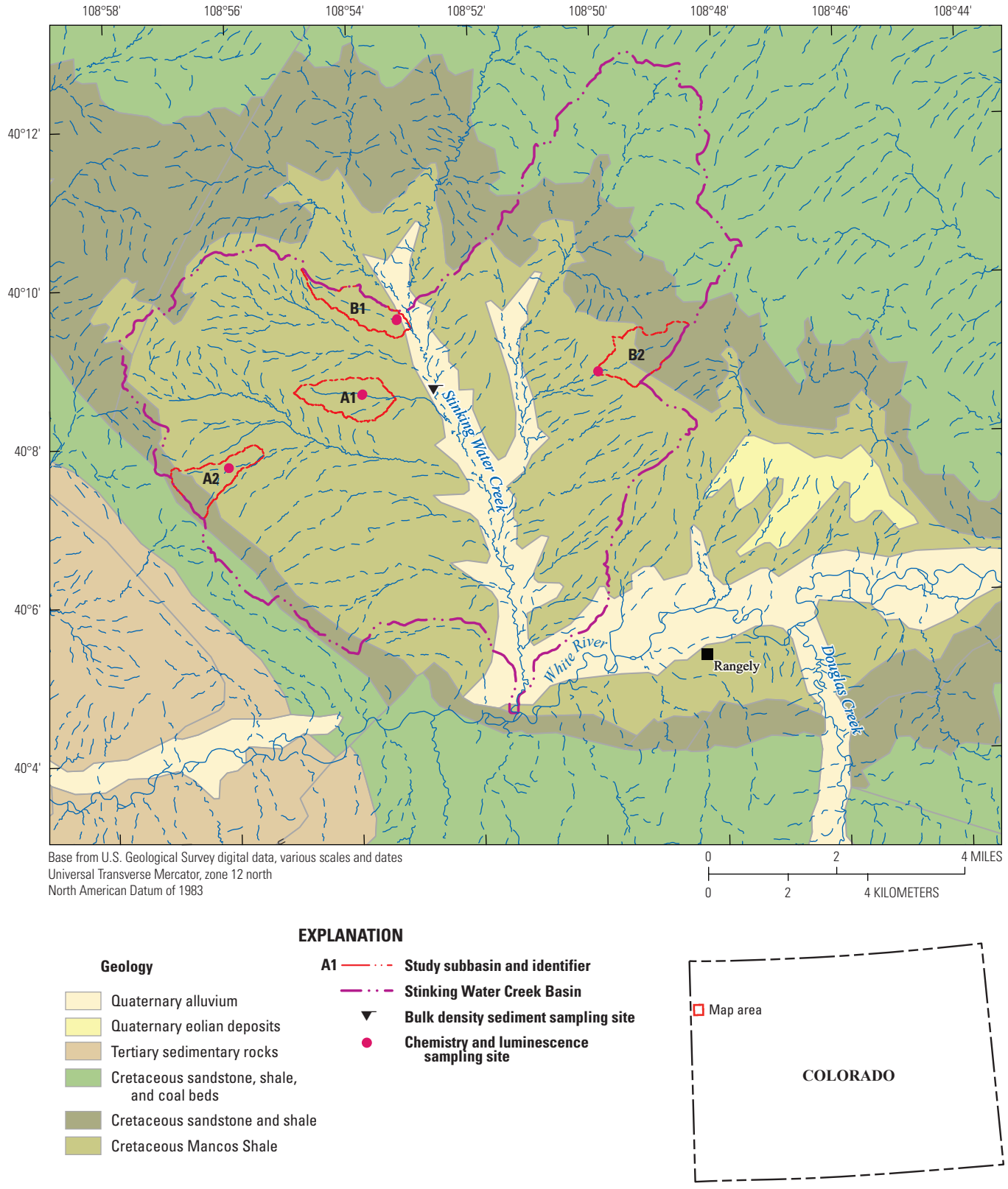


Figure 2. Locations of four selected subbasins, bulk density sediment sampling site, geology of Stinking Water Creek, near Rangely, Colorado. Geology modified from Tweto (1979).

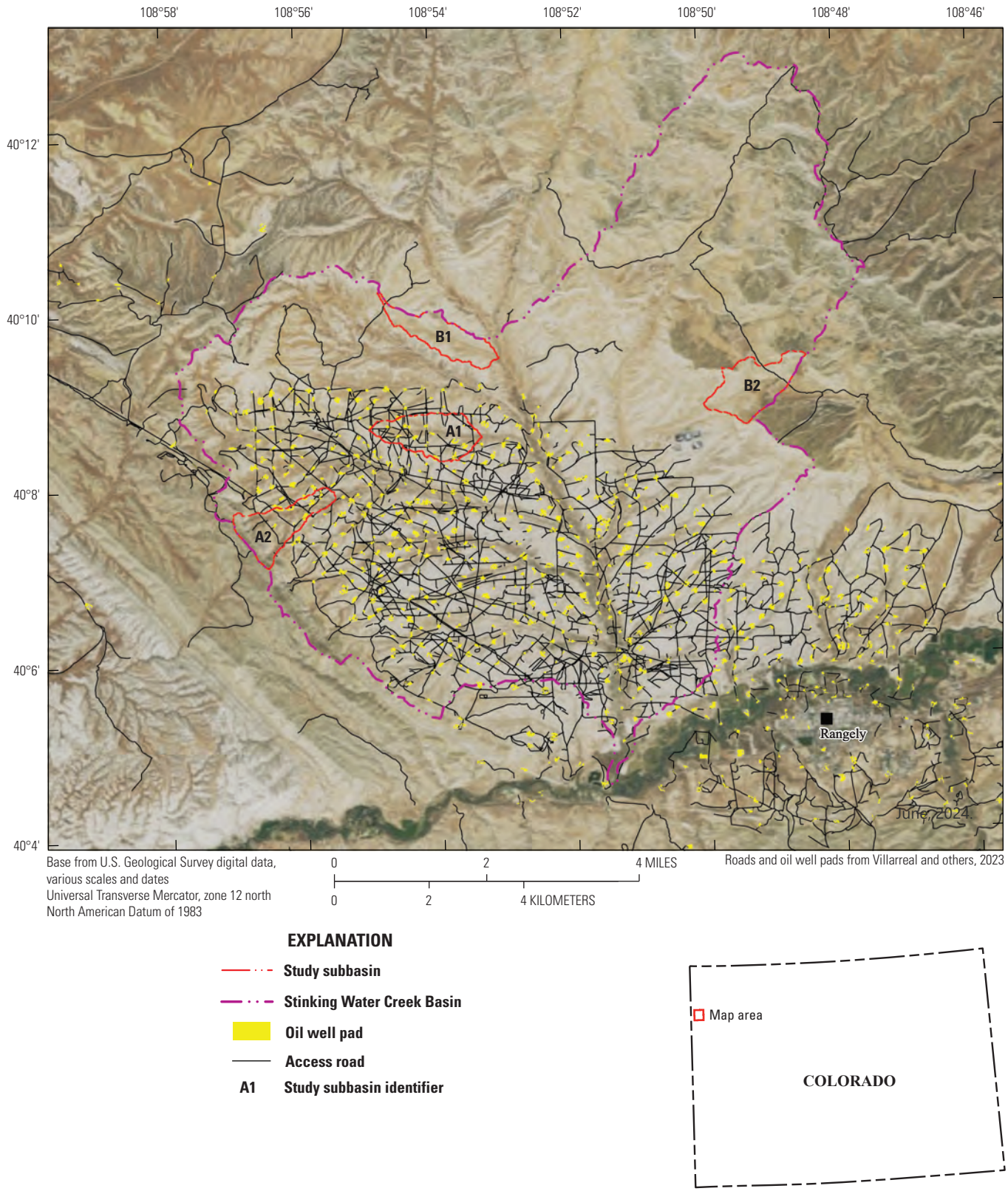


Figure 3. Roads and oil well pad locations in Stinking Water Creek Basin near Rangely, Colorado.

Arroyo System Geomorphology and History

An arroyo is a dry creek, streambed, or gulch that temporarily or seasonally fills and flows after sufficient precipitation, with flash floods common following thunderstorms. Arroyos are often described as a series of incision and fill cycles brought about by processes that change sediment supply or water within the system (Schumm and others, 1984) and generally are largely composed of very fine-grained sediment that is easily eroded. Arroyo systems are coupled processes between hillslope delivery of sediments and surface-water runoff that determine erosion, transport, and deposition. Changes in basin characteristics can alter streamflow and the delivery of sediment, affecting sediment storage within a system (Griffin and Friedman, 2015). Drawing from the geomorphic concepts of the graded stream (Mackin, 1948) and regime theory (Leopold and Maddock, 1953), channel adjustment will continue until continuity between sediment supply and fluvial sediment transport is restored. These cycles can occur simultaneously, or at different times across the basin (Schumm and Hadley, 1957).

Other processes can contribute to localized changes in sediment storage. The steep, often vertical walls of an arroyo can reach a point of instability, where greater heights result in mass wasting of parts of the vertical walls into the streambed. Streambank erosion through undercutting or oversteepening (streambank height exceeding a maximum, stable height termed "critical bank height") is determined by sediment particle size, sorting, root structure, and soil moisture (Knighton, 1998; Simon and others, 2000; Rosgen, 2006). Arroyos are also prone to erosion in the subsurface. Soil piping, a term for the subsurface hollowing of sediments through transport and dissolution, can form subsurface flow networks similar to burrows or caverns that can eventually result in surface collapse, causing a steep-walled tributary to form (Parker and Jenne, 1967; Bryan and Jones, 1997). Localized oversteepening may occur in the main channel as well and can drive incision and subsequent erosion in an upstream direction (Schumm and Hadley, 1957).

The three primary geomorphic responses to changes in streamflow and sediment conditions are channel widening, channel deepening, and changes in plan-view form (Schumm and others, 1984). Channel widening often results from hydraulic forces, mass wasting, or a combination of both (Fischenich and others, 1989), whereas channel deepening (incision) often occurs because of decreased sediment supply or increased channel slope, streamflow, or velocity (Simon and Darby, 1997; Bledsoe, 1999). Changes in plan-view form (changes in channel position and shape) include the migration of meandering bends and changes in sinuosity. These alterations are often linked to changes in channel bed slope (Lane, 1954). Channel evolution models represent a typical sequence or progression of changes within a stream system that occur in response to a perturbation in the dynamic equilibrium (Schumm and others, 1984). The channel evolution model describes the physical conditions and dominant processes that are active in the stream, at given points in time and as a progression of changes that occur in sequence. For example, a typical idealized sequence that follows erosion within a reach is (1) single-thread equilibrium condition; (2) incision and isolation of floodplain; (3) oversteepening of streambanks, increased streambank instability, channel widening with continued incision; (4) channel aggradation with continued widening; and (5) return to quasiequilibrium at new, lower elevation (Schumm and others, 1984; Simon, 1989; Simon and Downs, 1995).

Numerous arid and semiarid areas in the southwestern United States experienced rapid arroyo entrenchment between the late 1800s and early 1900s. Many historical accounts attributed the erosion to the effects of human activity disturbances such as grazing, roads, railroads, and irrigation and flood control structures (Antevs, 1952; Aby, 2017); however, examination of stratigraphic exposures has revealed evidence of multiple prehistoric cycles of arroyo incision and filling (Waters and Haynes, 2001; Hereford, 2002; Harvey and others, 2011; Summa-Nelson and Rittenour, 2012). Climate, drought, flooding, vegetation, and land disturbance may all affect arroyo erosion (Antevs, 1952; Bull, 1997; Waters and Haynes, 2001).

Depositional (or fill) terraces are preserved flat areas that represent the surface of an old floodplain or streambed. These terraces can form in response to changes in flow regime or changes in equilibrium such as alterations in sediment supply (Bull, 1990). Higher elevation terraces are older in age than lower elevation terraces according to the theory that incision carves downward into the arroyo or stream through time. When base level changes and the channel system begins to incise or erode, pieces of these once wide and flat floodplains are preserved as flat-topped terraces of varying elevation on the landscape.

Womack and Schumm (1977) studied terraces on Douglas Creek, a tributary to the White River southeast of Stinking Water Creek (fig. 2). By comparing tree-ring records, historical aerial photographs, the position of trees, and a homestead relative to the stream, they concluded episodic erosion (or incision) took place after 1900 and represented a complex response to overgrazing during the 1880s. Additional studies of Douglas Creek showed evidence of cyclical arroyo incision and aggradation during the Holocene Period, with the most recent incision occurring from around 1880 to 1940 (Hayden, 2008; Graham, 2015). No previous work has been done to date terraces and the timing of incision in the Stinking Water Creek Basin nor along the White River near Rangely.

Methods

Examination of historical records and OSL dating provided information about the previous land-use change and arroyo formation in Stinking Water Creek. Surveying, remote sensing, and sediment sample analysis were used to characterize geomorphology and sediment chemistry in the four subbasins. Sediment transport models were used to estimate hillslope and road erosion potential. Comparisons between subbasins were used to infer differences in the effects of land use.

Historical Aerial Photographs

A series of aerial photographs was used to analyze land-use change and channel changes in the study area. Historical photographs of all four subbasins were compiled and downloaded from EarthExplorer (U.S. Geological Survey, 2016), which resulted in photographs from seven time periods (1953, 1962, 1982, 1993, 1999, 2009, and 2013). Other historical records (Gale, 1908; Colorado School of Mines, 2005) were used to assess land-use change prior to 1953.

The aerial photographs were imported into Esri ArcMap 10.3.1 (Esri, 2015) to perform the land-use analysis. Most of the aerial photographs collected prior to 2000 were not georeferenced, which was required to make any qualitative analysis through history. Thus, the Georeferencing toolbox in Esri ArcMap 10.3.1 (Esri, 2015) was used to georeference all aerial photographs not georeferenced in their native format. Approximately 25 control points were used for each aerial photograph to achieve a root-mean squared error of less than 10 m. The methodology for establishing control points is discussed in the "Real-Time Kinematic Global Navigation Satellite Systems Survey and Uncrewed Aerial Systems" section of this report.

The Create Features tool in the Editor toolbox of Esri ArcMap 10.3.1 (Esri, 2015) was used to develop shapefiles of polygons and lines that represent landscape disturbances and channel location, respectively. Landscape disturbances such as roads, oil and gas pipelines, oil well pads, and constructed ponds were traced based on visual evidence in the georeferenced historical aerial photographs to generate polygons of landscape disturbances. The polygons were then compiled into the seven time periods and types of landscape disturbance before calculating the total area of each disturbance by using the Calculate Geometry tool in Esri ArcMap 10.3.1 (Esri, 2015). The main channel of each subbasin was traced based on visual evidence in the georeferenced historical aerial photographs to generate lines of the channel location.

Real-Time Kinematic Global Navigation Satellite Systems Survey and Uncrewed Aerial Systems Survey

A real-time kinematic (RTK) Global Navigation Satellite System (GNSS) survey completed in 2016 generated a series of control points used to georeference the topographic data collected from the uncrewed aerial system (UAS). A piece of rebar was driven into the ground, and approximately 1-m by 1-m black and white aerial targets were centered and secured above the rebar, which was then surveyed to determine its exact position using the standardized methodology in Rydlund and Densmore (2012). As a result, the topographic data collected from the UAS platform were referenced to the same datums as the RTK GNSS survey.

A GNSS survey uses the U.S.-based Global Positioning System (GPS) satellite network and the Russian GLObal NAvigation Satellite System satellite network, whereas a GPS survey uses only the GPS satellite network (Rydlund and Densmore, 2012). The RTK GNSS survey was referenced to Universal Transverse Mercator Zone 12 north projection, the North American Datum of 1983 (NAD83), and the North American Vertical Datum of 1988 (NAVD88), Geoid 2012B. Throughout this report, locations and elevations are presented relative to these datums and projection.

An RTK GNSS survey uses a static base station that continuously collects data throughout the survey and transmits the static position to mobile rovers, which are operated by individual surveyors who travel across the study area collecting data. The control and calibration points from the subbasins were surveyed using a Trimble R8 GNSS base receiver equipped with a Trimble TDL450H radio or the internal radio in the Trimble R8 GNSS base receiver and as many as three mobile rovers (depending on day), with each consisting of a Trimble R8 GNSS receiver and a Trimble TSC3 data controller or a Trimble TSC2 data controller mounted on a 2-m survey rod.

Data collected throughout the study were submitted to the National Geodetic Survey's Online Positioning User Service for processing (National Geodetic Survey, 2017). Afterwards, the survey data collected by the mobile rovers were recomputed to reflect the solution correction through a shift in the northing, easting, and elevation.

Surveys by UAS equipped with a high-resolution digital camera were completed for the four subbasins in 2016 (Preston and others, 2021). Structure from motion techniques (Ullman, 1979) and overlapping images from the UAS survey were used to create a dense point cloud, georectified orthoimage with resolution of 3.87 centimeters, and digital elevation model (DEM) for each of the four subbasins. Digital terrain models (DTMs) were exported at the same extent and resolution of the orthoimagery by reclassifying the dense point cloud as either bare ground or other (vegetation, oil and gas infrastructure) and interpolating the

land surface between bare ground points. Because vegetation caused the DTMs to be higher than the DEM in some areas, final surface models were created by merging the DTMs with the DEMs for all areas where the DTM was greater than the DEM. Files and detailed methodology are provided in Preston and others (2021).

Channel Morphology

Using the final surface models described in the previous section, and ArcMap software (Esri, 2020), flowlines were created for the four subbasins by extracting the lowest elevation points (thalweg) from the DEM and cross-section profiles were extracted at intervals of 25 m. The positions of upper and lower terrace surfaces were determined based on field observations, visual inspection of aerial imagery, and the cross-section profile plots (fig. 4). Cross-section profiles were not included in the analysis if they were altered (for example, areas that looked dammed or bulldozed on aerial images) or if the cross section plotted parallel to the channel rather than perpendicular. A lower terrace was not present at every cross section. The R statistical software (R Core Team, 2019a) was used to calculate cross-section characteristics (area, width, depth, and width-to-depth ratio) for the upper and lower terraces. Upper terrace cross-section characteristics were representative of the entire arroyo (upper terrace to streambed), whereas lower terrace cross-section characteristics were representative of the inner channel (lower terrace to streambed), and the lower terrace represented the active channel floodplain.

Cross-section characteristics were first evaluated with the Kruskal-Wallis test (Helsel and others, 2020) to determine if differences existed between groups (subbasins). When significant differences were indicated (α=0.05), the pairwise Wilcoxon rank sum test, a nonparametric multiple comparison test (Helsel and others, 2020), was used to determine which groups differed. The pairwise Wilcoxon rank sum test was used with the Benjamini and Hochberg (1995) correction (Helsel and others, 2020) using the R package stats (R Core Team, 2019b) to determine significant differences (α=0.05) in a pairwise comparison.

In addition, bankfull channel morphology characteristics based on the 0.10 annual exceedance probability (Q_{10}) peak streamflow obtained from StreamStats (U.S. Geological Survey, 2019) were determined for a subset of cross sections in each subbasin. This analysis was done to allow comparison of the Stinking Water Creek channels with an assessment of Q_{10} bankfull characteristics for ephemeral streams in the Grand Valley, western Colorado, which have similar geologic setting and climate to the Stinking Water Creek Basin. Homan (2024) assessed the Grand Valley streams to characterize stream channel stability and identify mechanisms affecting erosion. Refer to Homan (2024) for a description of methods for determining Q_{10} streamflows and associated sinuosity and shear stress.

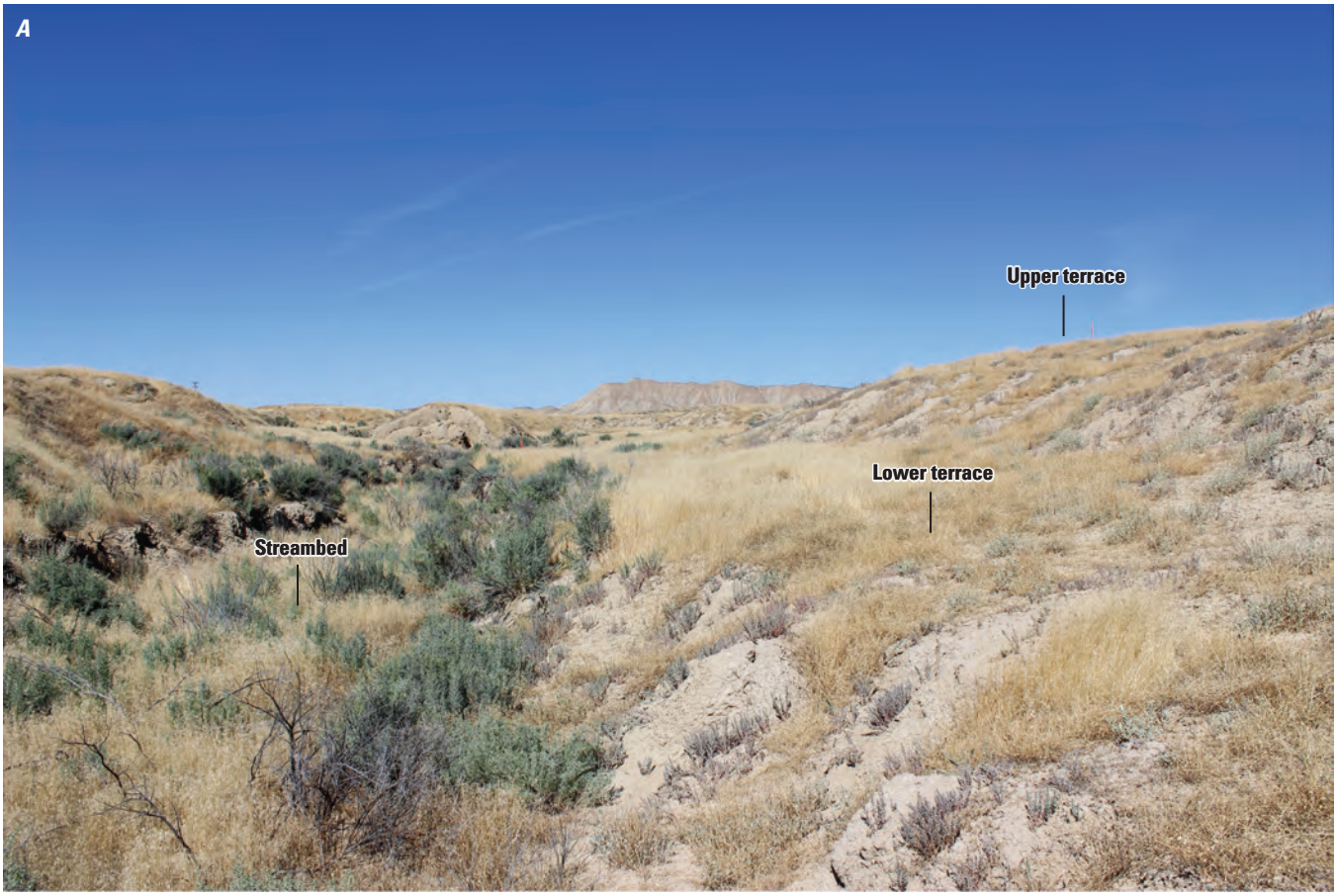
Sediment Chemistry, Dating, and Density

In each of the four subbasins, one sediment sampling site for sediment chemistry and OSL was selected where two terraces were present above the streambed to target geomorphic surfaces that represent depositional settings (fig. 2). Dry sediment samples were collected from a site along the main stem of Stinking Water Creek for determination of dry bulk density.

Sediment Chemistry

Sediment samples were collected using stainless steel and plastic utensils into acid-rinsed high density polyethylene containers. Samples were field sieved to less than 2 millimeters and freeze dried in the laboratory. For salinity determination (also referred to as total dissolved solids or TDS), samples were processed following procedures modified from Laronne and Schumm (1982). Sediment pastes were prepared by combining a known mass of freeze-dried sediment (approximately 20 grams) with a known volume of deionized water (approximately 200 milliliters). The mixtures were stirred, allowed to sit for 1 hour, stirred, allowed to sit for at least 12 hours, and stirred again. The mixtures were filtered through 25-micrometer filter paper before filtering through 0.45-micrometer syringe filters. Using residue on evaporation techniques, water-soluble leachates were analyzed for TDS at the USGS National Water Quality Laboratory in Denver, Colorado (Fishman and Friedman, 1989). The resulting concentrations in milligrams per liter (mg/L) were related to the mass of sediment and volume of dilution water to arrive at concentrations of salts in milligrams per kilogram of dry sediment (mg/kg).

Selenium speciation in sediments was obtained by using sequential extractions, which provide the best available means for studying selenium speciation in solid phases (Zawislanski and others, 2003). Pronounced differences in solubility and bioavailability of selenium species have led to the development of sequential-extraction protocols allowing quantification of selenium abundances in operationally defined fractions (Kulp and Pratt, 2004). Sequential extraction of selenium from the samples followed protocols described by Kulp and Pratt (2004). The sequence of extractions includes (1) water-soluble selenium, (2) exchangeable selenium, (3) base-soluble selenium, (4) elemental selenium, and (5) acetic-acid-soluble selenium (carbonate). Selenium analyses were completed using hydride generation atomic absorption spectroscopy at the USGS Geology, Geophysics, and Geochemistry Science Center Laboratory in Denver, Colorado (Briggs and Crock, 1986).



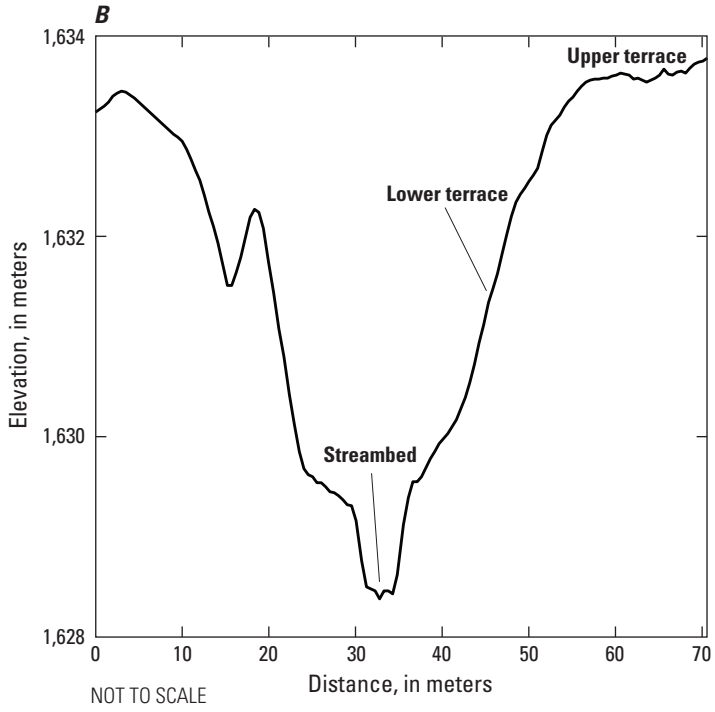


Figure 4. Stinking Water Creek subbasin A1 sampling location showing *A*, photograph of geomorphic surfaces, and *B*, plot of a cross-section profile. Photograph by Cory A. Williams, U.S. Geological Survey.

For quality assurance and quality control, duplicate extractions were prepared for one TDS sample. The difference between TDS results was 5 percent (31 mg/L; Gidley and others, 2026). One duplicate sample was submitted for sequential extraction of selenium. For the sequential extraction results, the differences were (1) 3.5 percent (0.04 micrograms per liter), (2) 22 percent (0.38 micrograms per liter), (3) 8 percent (1.37 micrograms per liter), (4) 43 percent (0.27 micrograms per liter), and (5) 20 percent (0.36 micrograms per liter; Gidley and others, 2026).

Optically Stimulated Luminescence Dating

The OSL dating techniques calculate the amount of time that has passed since sediments were exposed to light. As sediments are buried, exposure to ionizing radiation from surrounding sediment and cosmic radiation causes electrons to become stored in quartz and feldspar grains and accumulate through time (Nelson and others, 2015). The amount of radiation received is based on the location, elevation, and burial depth; radioisotope concentrations (potassium, rubidium, thorium, and uranium); and moisture content of the sediments (Nelson and others, 2015; Mahan and others, 2023). When the minerals are exposed to light, electrons are released along with a luminescence signal (photon), and the time since last exposure is proportional to the amount of radiation received and the intensity of the luminescence signal (Nelson and others, 2015; Mahan and others, 2023).

Use of OSL techniques can date sediments from a wide range of ages, typically hundreds to thousands of years (Nelson and others, 2015). In fluvial settings, the ages determined by OSL can bracket periods of incision and aggradation (Pederson and others, 2006; Summa-Nelson and Rittenour, 2012; Hayden-Lesmeister and Rittenour, 2014). Slope is an important control on arroyo formation, but a fluvial system at a slope threshold will not entrench until there is a flood large enough to exceed the transport capacity needed for incision (Townsend and others, 2019). Thus, OSL ages often measure when a slope stability threshold was exceeded, forming paleochannels for arroyo development.

Difficulties with interpreting the OSL ages arise when quartz grains are partially bleached, meaning the light exposure was not sufficient to fully reset the luminescence signal on its last transport path. This causes overestimation of ages, because the sediment does not reflect a zero depositional age (Olley and others, 1998; Wallinga, 2002; Medialdea and others, 2014). Partial bleaching can be caused by transport in highly turbid flows that light cannot penetrate (Smedley and Skirrow, 2019), very short pathways of transport, or mixing of soft sediments of varying depositional histories. These conditions are common in arid and semiarid environments (Porat and others, 2001; Harvey and others, 2011; Summa-Nelson and Rittenour, 2012). Additionally, complications arise where changes to channel form occur without preservation of deposits within the sequence. Fine-grained sediments can be washed out of a basin (Antevs, 1952) instead of being preserved as deposits available for OSL dating.

Samples for OSL dating were collected in September 2015 and November 2016 at the same locations where sediment chemistry samples were collected. Sediment samples were collected from pits (depth of 0.3 m below the terrace surface or streambed) or excavated walls in the dark (under blackout fabric) by driving a metal tube into the sediment (Nelson and others, 2015). Bulk sediment samples were collected at each sampling location and placed in air-tight containers for dose rate calculations and determination of water content and concentrations of radioisotopes (Nelson and others, 2015). The OSL analysis was done at the USGS Luminescence Dating Laboratory in Denver, Colorado, following standard protocols (Mahan and others, 2015; Nelson and others, 2015). The systematics of OSL techniques are well known and replicated in many laboratories (Thomsen and others, 2008; Steffen and others, 2009; Buylaert and others, 2011). In the laboratory, subsamples for equivalent dose measurements (natural luminescence accumulations) were obtained from the center of the core tubes.

In subdued orange-light conditions in the laboratory, 4-molar hydrochloric acid and 45-percent hydrogen peroxide were applied to the samples for OSL dating, followed by wet sieving isolated grains with diameters of 63–250 microns. Heavy minerals and some feldspars were separated from the quartz with a Frantz magnetic separator using a high (1.5 ampere) current. A brief separation using heavy liquid with 2.56 grams per milliliter density was enough to float the potassium-rich feldspars for collection. Quartz was collected following the separation and subsequently etched with concentrated (48 percent) hydrofluoric acid for 40 minutes to dissolve grain rinds affected by alpha particles and rid the sample of any remaining feldspars. This procedure was followed by treatment with 6-molar hydrochloric acid to remove any precipitated fluorides. Steel target discs were dabbed with a small circle of silica spray, and a single-grain-thick layer of refined grains was dispersed onto the steel discs. These discs were then loaded onto a carousel, ready for OSL analyses. About 30–40 aliquots were measured to ensure the most reliable statistical trends (Rodnight, 2008). A single aliquot regenerative dose protocol (Wintle and Murray, 2006) was used to determine the equivalent dose for each quartz aliquot using continuous-wave OSL. Aliquots were as small as possible for each measurement, generally 25–50 grains per disc.

Dose rates (D_R) were calculated based on concentrations of potassium, rubidium, uranium, and thorium, which were measured by inductively coupled plasma mass spectrometry following standard USGS procedures (Taggert, 2002) and gamma spectrometry (Nelson and others, 2015). The cosmic-ray component of the D_R was estimated for each sample as a function of depth, elevation, and geomagnetic latitude and added to the total dose rate (Prescott and Hutton, 1994). The cosmic D_R was combined with the alpha, beta, and gamma dose rates to give the total D_R. The total D_R was corrected for the effects of grain size and water content. The alpha contribution was disregarded, because the quartz was etched in hydrofluoric acid, leading to removal of the outer edges of the mineral.

The bulk sediment was generally coarse grained with a field moisture reading of 2–12 percent. After drying, the sediment was weighed, reintroduced to water, and centrifuged to simulate compaction. Next, the water was poured off, and the sediment was reweighed to obtain an approximate potential total water content, referred to hereafter as saturation moisture. The D_R and ages were calculated using approximately 25 percent of the saturation moisture to simulate average yearly precipitation, because the samples were collected from consistently dry environments but subject to periodic high volumes of water. OSL age uncertainties are given at the 68-percent (1-sigma) confidence level.

Sediment Density

Five sediment samples were collected from one site on the main stem of the Stinking Water Creek where three terrace surfaces were present (fig. 2) for determination of dry bulk density: three from the first terrace above the streambed, one from the second terrace above the streambed, and one from the third terrace above the streambed. The samples from the first terrace above the streambed were collected at different locations on that surface (one from the left bank, one from the right bank, and one from the area between the main stem channel and a tributary). At each location, vegetation and the top layer of sediment were cleared before driving a cylinder with a volume of 90.59 cubic centimeters into the sediment. Cores were collected so that the cylinder was filled completely without compacting the sediment. In the laboratory, each core was placed in a preweighed drying tin and dried at 105 degrees Celsius for at least 12 hours. The dry sediment weight was divided by cylinder volume to obtain density in grams per cubic centimeter (U.S. Department of Agriculture, 2001).

Sediment Transport Models

Sediment transport was estimated by using the WEPP model, which is a process-based sediment transport model that evaluates hillslope erosion potential based on equivalent gradient, soil and vegetation properties, and rainfall properties (Flanagan and Nearing, 1995). Sediment erosion is approximated, and routing of sediment is represented in deposition and scour along the surface. Comparisons of hillslope production are made by simulating many years of transport to capture the variability of storm occurrence and intensity to arrive at long-term average transport rates as well as transport extremes (Flanagan and Livingston, 1995; Flanagan and others, 2013). The suitability of the model is limited by the size of the modeled area, and the model can be applied to basins 260 hectares and smaller (Flanagan and Nearing, 1995; Flanagan and others, 2013).

WEPP modeling to estimate hillslope sediment loss was completed using the WEPPcloud online interface, which can automate retrieval and processing of the required input datasets (Lew and others, 2022). Input datasets for elevation, vegetation, soils, and climate were all retrieved and generated within WEPPcloud. Channels and hillslopes were delineated from elevation data by the Topographic Parameterization program (TOPAZ; Garbrecht and Martz, 1997). The minimum channel length was 60 m, and the critical source area was 4 hectares. These values were reduced from the default values of 100 m and 10 hectares, respectively, to represent the small subbasins (Kampf and others, 2020; Lew and others, 2022). The 2016 National Land Cover Database (Dewitz, 2019) was selected as the source of data to summarize the land cover for each hillslope. Similarly, soil types were summarized for each hillslope using Soil Survey Geographic Database (SSURGO) data (Reybold and TeSelle, 1989). Climate information was generated using the Parameter-elevation Regressions on Independent Slopes Model (PRISM; Daly and others, 2008) with data from the National Climatic Data Center's Rangely, Colo. station. One WEPP run with 100 years of simulation was completed for each of the four subbasins.

WEPP:Road, a WEPP model interface, was used to estimate runoff and sediment delivery from roads (Elliott, 2004). The WEPP:Road Batch webservice tool (U.S. Department of Agriculture Forest Service, 2008) allowed batch simulations for many road segments (Elliot, 2021). Batch input files contain a list of road segments and their associated design, surface type, traffic level, percentage of rock fragment, gradient, length, and width as well as fill and buffer gradient and length. The road polygons delineated based on 2013 aerial photographs (described in the "Historical Aerial Photographs" section of this report) were used as the road segments for the batch simulations. In ArcMap version 10.3.1 (Esri, 2015), buffer length was determined by measuring the distance from a road segment to the nearest stream channel, and a DEM (U.S. Department of Agriculture, 2004) was used to determine the road and buffer gradients (slopes). The road design, surface type, and traffic level were assigned based on visual inspection of aerial imagery. For all road segments in all four subbasins, rock fragment was set to 0 percent, fill gradient was 50 percent, and fill length was 0.3 m. Batch simulations for all four subbasins used climate data for the Rangely, Colorado, climate station, clay loam soil, and 100 years of simulation.

Incision Rates and Load Estimates

The median incision rate from the upper terrace to the streambed was determined for each subbasin. Incision rates were calculated for each extracted cross section (described in the "Channel Morphology" section of this report) using the OSL ages and elevation differences between the upper terrace and the streambed. Total changes in channel volume from the upper terrace to the streambed were computed for the four subbasins using the cross-section areas. For each cross section, the area was multiplied by half the linear distance between the previous cross section and the next cross section to result in a volume for the channel reach. Volume change through time was determined by dividing the change in volume by the difference in age between surfaces. The volume was then

converted to mass of sediment, salts, and selenium, using the median sediment density (same value for all four subbasins) and concentrations of salinity and selenium determined from prepared sediment-water extracts. Combining the output from WEPP Hillslope (hillslope soil loss) and WEPP:Road (sediment leaving the road buffer) with the mass of sediment associated with volume change resulted in a sediment load for each subbasin. Salinity and selenium loads were also computed using the minimum, median, and maximum concentrations for all four subbasins.

Results

Data associated with this report are available in USGS data releases (Preston and others, 2021; Gidley and others, 2026; Mahan and others, 2026).

Timeline of Land-Use Change

Examination of aerial photographs and other historical sources allowed for characterization of land-use change and disturbances in the study area. The percentage of disturbed area was low in all four subbasins in 1882 and remained low through the early 1940s (fig. 5). The amount of disturbed area in subbasins A1 and A2 then increased through the 2000s as energy development began and expanded. In 2013, the types of disturbance present in the subbasins included roads, oil well pads, oil and gas pipelines, and constructed ponds (fig. 6). The disturbed area in subbasins B1 and B2 remained low (less than 5 percent of subbasin area; fig. 5).

Channel Morphology

The Kruskal-Wallis statistical test indicated at least one subbasin was different in terms of cross-section area, width, depth, and width-to-depth ratio in the upper and lower terrace datasets ($\alpha = 0.05$); therefore, the pairwise Wilcoxon rank sum test was used to determine how subbasins differed ($\alpha = 0.05$; Helsel and others, 2020).

Results for the upper terrace dataset showed differences between subbasins, although the subbasins were not always grouped by land use (fig. 7). In terms of cross section depth, subbasins A1 and A2 were grouped and subbasins B1 and B2 differed, with smaller median depths in the A subbasins than in the B subbasins. Median width-to-depth ratios were greatest in A1 and smallest in B2. Cross-section area and width were larger in the downstream subbasins (A1 and B1, whose outlets are near the main stem of Stinking Water Creek) compared to the corresponding upstream subbasins (A2 and B2, which are located at higher elevation and have steeper slopes and outlets farther from the main stem, fig. 2).

The lower terrace dataset showed differences between land use in terms of cross-section area and depth (fig. 8). For both measurements, the A subbasins were grouped and generally smaller than the B subbasins, which were also grouped. Cross sections were wider in the downstream subbasins than in the upstream subbasins; the values were similar for the A1 and B1 subbasins, and the A2 and B2 subbasins were similar. The A subbasins were alike in terms of width-to-depth ratio; however, subbasin A2 was also grouped with subbasin B1. As with the upper terrace dataset, median width-to-depth ratios were greatest in subbasin A1 and smallest in B2, which differed from the other subbasins.

Comparison of Q_{10} channel characteristics shows some similarities between the Stinking Water Creek subbasins and ephemeral streams in the Grand Valley, western Colorado. Homan (2024) described geomorphic characteristics for 48 ephemeral streams in the Grand Valley to assess stream channel stability and identify mechanisms affecting erosion. The Grand Valley cross sections were classified as stable (no evidence of active erosion) or active (evidence of active erosion) based on field observations, and a subset of the active cross sections were classified as incising or widening. The study determined stable cross sections generally had smaller drainage area, lower sinuosity, lower shear stress, and greater width-to-depth ratio compared to actively eroding cross sections (Homan, 2024). Within the active cross sections, those with lower sinuosity were more likely to be incising rather than widening (Homan, 2024). The Stinking Water Creek subbasins are much smaller than the Grand Valley basins (Homan, 2024), and there are differences in the range of values determined for channel characteristics. However, some similar patterns are apparent when comparing a subset of cross sections. For the Stinking Water Creek cross sections, subbasins A1 and A2 had similar drainage areas but higher sinuosity, less shear stress, and greater width-to-depth ratio than subbasins B1 and B2 (table 1).

Sediment Density and Chemistry

Bulk density was consistent across the five sediment samples (table 2), and the median value was 1.36 grams per cubic centimeter.

TDS concentrations ranged from 360 (sample subbasin B2 lower terrace) to 6,330 mg/kg (sample subbasin A2 lower terrace; table 3). The TDS concentrations varied by geomorphic surface in each subbasin and generally increased from the streambed to the upper terrace. Subbasin B2 had the overall lowest values on the terraces (490 mg/kg upper terrace and 360 mg/kg lower terrace) with the streambed markedly higher at 2,000 mg/kg. Subbasin B1 had the overall highest mean (3,360 mg/kg) and median (4,020 mg/kg) values but a low streambed value of 690 mg/kg.

Selenium concentrations (sum of extracted selenium) also varied between geomorphic surfaces in the four subbasins. Both the highest (0.36 micrograms per gram [µg/g], lower terrace) and lowest selenium concentrations (0.10 µg/g, upper terrace) were from subbasin A2 (table 4). The highest overall mean and median however, was from subbasin B2 with a value of 0.31 µg/g; the other subbasin mean and median values were 0.17–0.23 µg/g.

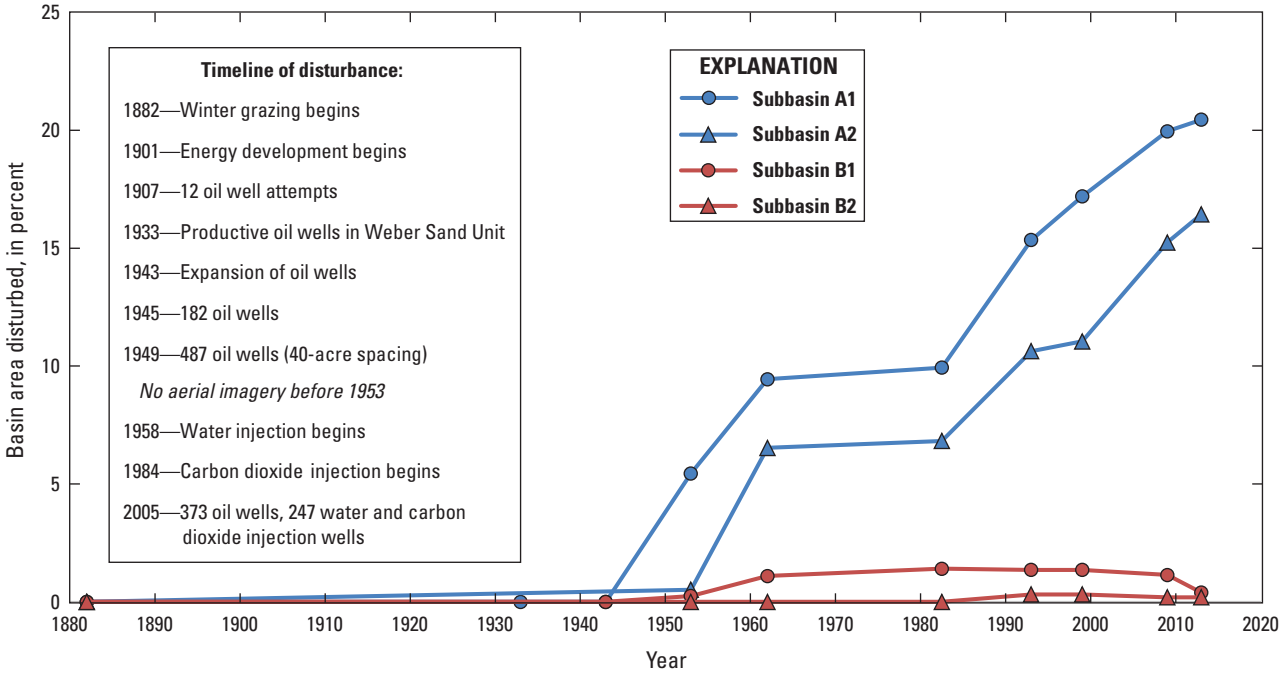


Figure 5. Percentage of disturbed area in four selected subbasins of Stinking Water Creek near Rangely, Colorado, 1882–2013. Disturbance types and areas were determined from georeferenced aerial photographs (available for 1953–2013; U.S. Geological Survey, 2016) and other historical records (prior to 1953; Gale, 1908; Colorado School of Mines, 2005).

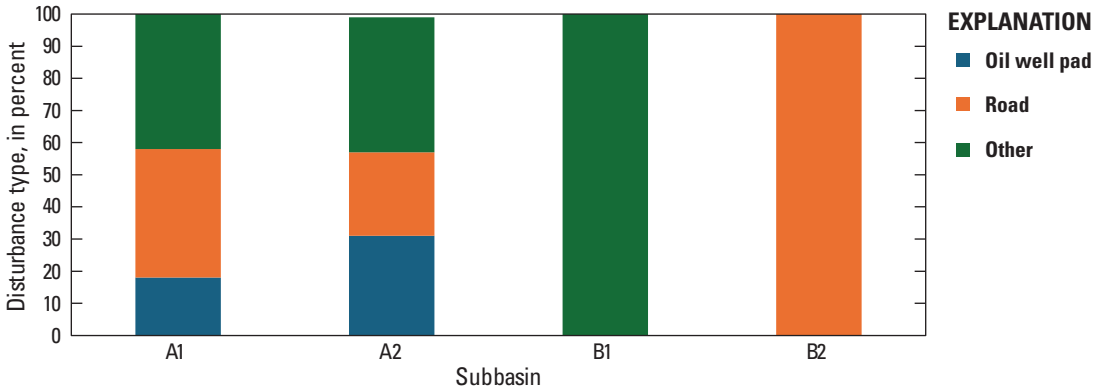


Figure 6. Disturbance types observed in 2013 aerial photographs of four selected subbasins of Stinking Water Creek Basin near Rangely, Colorado. Refer to figure 5 for the percentage of disturbed area in each subbasin. The other category includes oil and gas pipelines, constructed ponds, and other soil disturbances. Disturbance types were determined from georeferenced aerial photographs (available for 1953–2013) and other historical records (prior to 1953; Gale, 1908; Colorado School of Mines, 2005).

Table 1. Comparison of channel morphology characteristics for 0.10 annual exceedance probability (Q_{10}) streamflow determined for 48 ephemeral streams in the Grand Valley, western Colorado (Homan, 2024), and the Stinking Water Creek subbasins, near Rangely, Colorado (U.S. Geological Survey, 2019; fig. 2).

Channel characteristic	Grand Valley cross sections from Homan (2024)				Stinking Water Creek cross sections			
	Stable	Active	Incising	Widening	Subbasin A1	Subbasin A2	Subbasin B1	Subbasin B2
Number of cross sections	570	836	266	158	9	9	9	8
Median drainage area (square kilometers)	5.6	12.8	11.7	14	0.91	0.54	0.85	0.74
Median sinuosity	1.25	1.32	1.29	1.35	1.08	1.12	1.06	1.07
Median shear stress	46.1	67.6	74	72.6	174	186.5	209.7	250.7
Median width-to-depth ratio	13.6	8.8	8.68	7.84	15.8	11.4	8.2	5.0

Table 2. Bulk density of sediment samples collected on the main stem of Stinking Water Creek, near Rangely, Colorado (fig. 2).

[Data from Gidley and others (2026). g/cm³, gram per cubic centimeter]

Sample number	Description of geomorphic surface	Bulk density (g/cm³)
1	First surface above streambed	1.43
2	First surface above streambed	1.33
3	Second surface above streambed	1.36
4	Third surface above streambed	1.44
5	First surface above streambed	1.32
	Median value	**1.36**

Table 3. Total dissolved solids (TDS) concentrations of sediment samples from selected subbasins of Stinking Water Creek near Rangely, Colorado.

[Data from Gidley and others (2026). Samples were collected from one site in each subbasin, and soil-water extracts were prepared for analysis of TDS by residue on evaporation techniques (Fishman and Friedman, 1989). The mass of soil and the volume of the extract solution were related to the measured concentrations to obtain TDS concentrations in milligram per kilogram of dry soil (mg/kg)]

Sample location	TDS (mg/kg)
Subbasin A1	
Upper terrace	3,920
Lower terrace	1,360
Streambed	1,380
Mean	2,220
Median	1,380
Subbasin A2	
Upper terrace	2,740
Lower terrace	6,330
Streambed	460
Mean	3,180
Median	2,740
Subbasin B1	
Upper terrace	5,370
Lower terrace	4,020
Streambed	690
Mean	3,360
Median	4,020
Subbasin B2	
Upper terrace	490
Lower terrace	360
Streambed	2,000
Mean	950
Median	490

Table 4. Sequential selenium extraction concentrations of sediment samples from selected subbasins of Stinking Water Creek near Rangely, Colorado.

[Data from Gidley and others (2026). Selenium concentrations were measured following a sequential extraction procedure described by Kulp and Pratt (2004). The mass of soil and volume of extract solution were related to the measured concentrations to obtain selenium concentrations in microgram per gram of dry soil (µg/g). NaOH, sodium hydroxide; Na_2SO_3, sodium sulfite]

Sample location	Water-extracted selenium (µg/g)	Phosphate-extracted selenium (µg/g)	NaOH-extracted selenium (µg/g)	Na_2SO_3-extracted selenium (µg/g)	Acetate-extracted selenium (µg/g)	Sum of extracted selenium (µg/g)
Subbasin A1						
Upper terrace	0.02	0.01	0.08	0.01	0.02	0.14
Lower terrace	0.02	0.01	0.11	0.01	0.02	0.17
Streambed	0.04	0.02	0.19	0.01	0.02	0.29
Mean	0.03	0.01	0.13	0.01	0.02	0.20
Median	0.02	0.01	0.11	0.01	0.02	0.17
Subbasin A2						
Upper terrace	0.02	0.01	0.06	0.01	0.01	0.10
Lower terrace	0.02	0.05	0.25	0.01	0.03	0.36
Streambed	0.02	0.02	0.17	0.00	0.01	0.23
Mean	0.02	0.03	0.16	0.01	0.02	0.23
Median	0.02	0.02	0.17	0.01	0.01	0.23
Subbasin B1						
Upper terrace	0.03	0.01	0.08	0.00	0.01	0.14
Lower terrace	0.05	0.02	0.11	0.01	0.02	0.21
Streambed	0.02	0.03	0.21	0.01	0.03	0.29
Mean	0.03	0.02	0.11	0.01	0.02	0.21
Median	0.03	0.02	0.13	0.01	0.02	0.21
Subbasin B2						
Upper terrace	0.01	0.04	0.23	0.01	0.02	0.31
Lower terrace	0.02	0.03	0.25	0.01	0.03	0.33
Streambed	0.00	0.04	0.21	0.01	0.01	0.28
Mean	0.01	0.04	0.23	0.01	0.02	0.31
Median	0.01	0.04	0.23	0.01	0.02	0.31

Luminescence Dating

Of the ages presented, all collected from the upper terraces are older or within error of the lower, younger terraces, and any discussion on the youngest ages will use the year of luminescence measurement as 2020 (the zero year to calculate 160 years of a luminescence age to a Gregorian calendar year would be 2020–160 = A.D. 1860). Subbasin B2 had both the oldest (upper terrace, 8,330 plus or minus [±] 770 years) and youngest (streambed, 160 ± 10 years) sediment of all samples collected (table 5). Note, the subbasin B2 sampling site is in a sandy unit of the Mancos Shale, unlike the sampling sites in the other subbasins (fig. 2). In the three remaining subbasins, the streambed sediments were older than those collected from either of the terrace surfaces.

Sediment Transport Models

Overall, hillslope simulations from the WEPP model predicted more hillslope soil loss for the upstream subbasins (A2 and B2) compared to the corresponding downstream subbasins (A1 and B1; table 6).

Differences between energy development (subbasins A1 and A2) and rangeland grazing (subbasins B1 and B2) subbasins are evident in the results of the WEPP:Road simulations from the WEPP model. Subbasins A1 and A2 have more road area and road-related runoff and sediment loss than subbasins B1 and B2 (table 7).

Table 5. Optically stimulated luminescence quartz results for sediment samples from selected subbasins of Stinking Water Creek near Rangely, Colorado.

[Data from Mahan and others (2026). ppm, part per million; Gy/kyr, Gray per thousand years; Gy, Grays; %, percent; yr, year]

Sample location	Percent water content[1]	Potassium (weight percent)[2]	Uranium (ppm)[2]	Thorium (ppm)[2]	Total dose (Gy/kyr)[3]	Equivalent dose (Gy)	*n*[4]	Scatter (%)[5]	Age (yr)[6]
				Subbasin A1					
Upper terrace	4 (20)	1.98 ± 0.04	2.27 ± 0.27	8.79 ± 0.37	3.18 ± 0.12	3.05 ± 0.19	7 (15)	56	960 ± 70
Lower terrace	9 (28)	1.93 ± 0.05	2.47 ± 0.21	8.86 ± 0.29	3.20 ± 0.11	2.90 ± 0.22	6 (25)	27	910 ± 80
Streambed	10 (28)	1.61 ± 0.04	1.69 ± 0.14	6.68 ± 0.36	2.71 ± 0.10	12.5 ± 1.07	3 (15)	28	4,610 ± 440
				Subbasin A2					
Upper terrace	7 (26)	2.09 ± 0.05	2.21 ± 0.11	7.92 ± 0.32	3.24 ± 0.10	4.05 ± 0.72	4 (15)	88	1,250 ± 220
Lower terrace	2 (32)	1.89 ± 0.04	2.69 ± 0.23	8.04 ± 0.41	3.05 ± 0.12	2.08 ± 0.21	6 (25)	52	680 ± 70
Streambed	7 (33)	1.78 ± 0.05	2.24 ± 0.25	7.97 ± 0.48	3.05 ± 0.14	9.47 ± 1.03	5 (15)	45	3,110 ± 360
				Subbasin B1					
Upper terrace	8 (30)	2.16 ± 0.06	2.73 ± 0.33	9.34 ± 0.45	3.43 ± 0.13	3.34 ± 0.56	2 (7)	33	970 ± 170
Lower terrace	7 (33)	2.11 ± 0.04	2.57 ± 0.32	9.11 ± 0.44	3.39 ± 0.11	2.48 ± 0.27	3 (15)	75	730 ± 80
Streambed	12 (29)	1.79 ± 0.06	1.66 ± 0.13	6.56 ± 0.37	2.80 ± 0.12	12.5 ± 1.71	3 (15)	68	4,460 ± 640
				Subbasin B2					
Upper terrace	4 (31)	2.16 ± 0.07	2.13 ± 0.17	9.88 ± 0.47	3.47 ± 0.11	28.9 ± 2.5	2 (15)	14	8,330 ± 770
Lower terrace	3 (40)	2.30 ± 0.08	2.38 ± 0.19	9.56 ± 0.38	3.55 ± 0.10	7.11 ± 0.60	3 (15)	19	2,000 ± 180
Streambed	10 (39)	2.47 ± 0.08	3.08 ± 0.24	10.2 ± 0.58	3.91 ± 0.14	0.61 ± 0.04	7 (18)	27	160 ± 10

[1]Field moisture, with values in parentheses indicating the saturation moisture percentage. Ages were calculated using 25 percent of the saturation moisture.

[2]Analyses from inductively coupled plasma mass spectrometry (Dean, 2005). All errors were obtained with calibration standards.

[3]Includes cosmic doses and attenuation with depth calculated using the methods of Prescott and Hutton (1994). Cosmic doses were 0.30 Gy/kyr for all samples.

[4]Number of replicated equivalent dose estimates used to calculate the total. Values in parentheses indicate total number of measurements included in calculating the represented equivalent dose and age using the minimum age model. Analyzed by single aliquot regeneration on quartz grains.

[5]Defined as over dispersion of the equivalent dose values. Values greater than 35 percent are considered poorly bleached sediments.

[6]Dose rate and age for fine-grained quartz in the 90–125 micrometer range for all samples. Exponential plus linear fit used on equivalent dose, errors to one sigma.

Table 6. Water Erosion Prediction Project model results for Stinking Water Creek subbasins near Rangely, Colorado.

[Data from Gidley and others (2026). Model results are for 100 years of simulation. m^3/yr, cubic meter per year; t/yr, ton per year]

Model result	Subbasin A1	Subbasin A2	Subbasin B1	Subbasin B2
Mean annual precipitation volume (m^3/yr)	426,000	412,000	365,000	555,000
Mean annual total hillslope soil loss (t/yr)	1.5	7.5	2.1	10.0

Table 7. Water Erosion Prediction Project road input parameters and model results for Stinking Water Creek subbasins near Rangely, Colorado.

[Data from Gidley and others (2026). Model results are for 100 years of simulation. m, meter; km/km^2, kilometer per square kilometer; mm, millimeter; mm/yr, millimeter per year; t/yr, ton per year]

Parameter or result	Subbasin A1	Subbasin A2	Subbasin B1	Subbasin B2
Number of road segments	197	114	2	4
Design (number of segments)	Insloped, bare ditch (8); outsloped, rutted (189)	Insloped, bare ditch (24); outsloped, rutted (90)	Outsloped, rutted (2)	Insloped, bare ditch (4)
Surface and traffic (number of segments)	Native low (62); native none (135)	Graveled high (9); native high (1); native low (31); native none (69); paved high (4)	Native low (2)	Native low (4)
Mean road grade (percent)	5	8	8	14
Sum of road length (m)	27,079	16,486	282	697
Road density (length divided by basin area; km/km^2)	17.2	11.7	0.2	0.4
Mean road width (m)	14.6	17.7	3.0	4.3
Fill grade (percent)*	50	50	50	50
Fill length (m)*	0.3	0.3	0.3	0.3
Mean buffer grade (percent)	4	6	5	7
Mean buffer length (m)	23.8	25.0	99.4	49.4
Rock content (percent)*	0	0	0	0
Sum of mean annual rain runoff for all segments (mm/yr)	1,087.1	713.7	0	5.1
Sum of mean annual snow run-off for all segments (mm/yr)	2,047.2	1.188.7	5.1	22.9
Sum of mean annual sediment leaving road for all segments (t/yr)	71.3	145.7	0.3	2.9
Sum of mean annual sediment leaving buffer for all segments (t/yr)	25.6	42.7	0.004	0.1

*Same value used for all road segments.

Incision Rates and Load Estimates

Incision rates; channel volume changes; and sediment, salinity, and selenium loads were computed for the four subbasins by using cross-section area and volume, OSL ages, sediment bulk density, and constituent concentrations (table 8). Sediment, salinity, and selenium loads were determined by combining total sediment volume change within the channel and associated mass of salts and selenium with estimated soil loss output from WEPP models. The OSL age associated with the subbasin B2 streambed sample (160 ± 10 years) was used as the youngest streambed age for all subbasins because streambed ages in subbasins A1, A2, and B1 are older than the terrace sample ages (table 5).

Change in channel volume and associated mass of sediment were higher in the downstream subbasins (A1 and B1) compared to the corresponding upstream subbasins (A2 and B2). In general, subbasin B1 represented the largest mass of salts and selenium associated with the change in volume (table 8), as well as the largest mean annual loads of sediment, salinity, and selenium (table 9). The estimated incision rates and mean annual loads are affected by the number of years used in the calculation (age of upper terrace minus 160 years), which was similar for subbasins A1, A2, and B1; however, the age of the upper terrace in subbasin B2 was much older than in the other subbasins (table 5). Therefore, the loads estimated for subbasin B2 represent a similar mass of sediment but divided during a much longer time period. For ease of comparison, selected subbasin properties and results are summarized in table 10.

Table 8. Estimated incision rates, change in channel volume, and associated sediment, salt, and selenium mass results for Stinking Water Creek subbasins near Rangely, Colorado.

[Data from Gidley and others (2026). Mass of salt and selenium was computed at three levels: using the minimum concentration, median concentration, and maximum concentration for each subbasin. In each row, the highest value is indicated by *. mm/yr, millimeter per year; m^3, cubic meter; m^3/yr, cubic meter per year; t, metric ton; kg, kilogram]

Estimate based on change in channel volume	Subbasin A1	Subbasin A2	Subbasin B1	Subbasin B2
Number of years used to calculate incision rate	800	1,090	810	8,170*
Median incision rate (mm/yr)	5.2	3.0	6.8*	0.8
Total change in channel volume (m^3)	156,000	113,000	270,000*	158,000
Total sediment mass (t)	213,000	153,000	370,000*	215,000
Salt mass, minimum (t)	290*	70	250	77
Salt mass, median (t)	290	419	1,470*	110
Salt mass, maximum (t)	830	970	1,970*	430
Selenium mass, minimum (kg)	30	15	51	60*
Selenium mass, median (kg)	36	35	77*	67
Selenium mass, maximum (kg)	62	55	106*	71

Table 9. Estimated sediment, salinity, and selenium annual load results for Stinking Water Creek subbasins near Rangely, Colorado.

[Data from Gidley and others (2026). Annual loads of salinity and selenium were computed at three levels: using the minimum concentration (min), median concentration (median), and maximum concentration (max) for each subbasin. In each row, the highest value is indicated by *. ty/r, ton per year; kg/yr, kilogram per year]

Estimate based on change in channel volume and sediment transport models	Subbasin A1	Subbasin A2	Subbasin B1	Subbasin B2
Number of years used in calculations	800	1,090	810	8,170*
Mean annual sediment load (t/yr)	293	172	482*	60
Mean annual salinity load, min (t/yr)	0.398*	0.079	0.33	0.022
Mean annual salinity load, median (t/yr)	0.404	0.754	1.94*	0.029
Mean annual salinity load, max (t/yr)	1.15	1.09	2.59*	0.12
Mean annual selenium load, min (kg/yr)	0.051	0.016	0.083*	0.002
Mean annual selenium load, median (kg/yr)	0.062	0.036	0.13*	0.0023
Mean annual selenium load, max (kg/yr)	0.106	0.057	0.17*	0.0024

Table 10. Selected subbasin properties and results for Stinking Water Creek subbasins near Rangely, Colorado.

[Mean basin slope determined from StreamStats (U.S. Geological Survey, 2019)]

Subbasin	Relative location in Stinking Water Creek Basin (fig. 2)	Mean basin slope (percent)	Land use	Percentage of basin area disturbed, 2013 (fig. 5)	Channel morphology (fig. 7 and 8)	Luminescence ages (table 5)	Sediment transport (tables 6 and 7)
A1	Downstream (near main stem)	6	Energy development	20.5	Large width-to-depth ratios; Small cross-section area and depth	Streambed age older than terrace ages	Low hillslope sediment loss; High road sediment loss
A2	Upstream (farther from main stem)	21	Energy development	16.4	Large width-to-depth ratios; Small cross-section area and depth	Streambed age older than terrace ages	High hillslope sediment loss; High road sediment loss
B1	Downstream (near main stem)	8	Rangeland grazing	0.4	Small width-to-depth ratios; Large cross-section area and depth	Streambed age older than terrace ages	Low hillslope sediment loss; Low road sediment loss
B2	Upstream (farther from main stem)	23	Rangeland grazing	0.2	Small width-to-depth ratios; Large cross-section area and depth	Streambed age younger than terrace ages	High hillslope sediment loss; Low road sediment loss

Discussion

This study concentrated on six main topics surrounding the surface geology of four selected subbasins in Stinking Water Creek.

1. Historical records, such as aerial photographs, were compiled to describe the timeline of land-use change in the study area.
2. Imagery from UAS surveys was used to create a DEM from which cross sections were extracted to allow for comparison of channel morphology between the subbasins. Cross sections were also used to calculate the volume of the channels.
3. Samples were collected and analyzed to determine sediment density and the concentrations of TDS and selenium, which are water-quality constituents of concern. Density values were used to calculate the mass of sediment associated with the change in channel volume.
4. Samples were collected to calculate the age of terrace surfaces in the subbasins using OSL to place time controls when terraces would have been developed or modified.
5. WEPP and WEPP:Road models were used to simulate hillslope and road sediment loss for the four subbasins. These results were combined with the mass of sediment associated with change in channel volume to estimate the amount of sediment leaving each subbasin during arroyo incision.
6. Sediment, salinity, and selenium loads were estimated based on the sediment mass, salt and selenium mass, and luminescence ages.

Timelines and Effects of Land Use on Channel Morphology

Changes in antecedent conditions, hydrology and flow regime (and thus vegetation that anchors the sediment), and localized perturbations in channel form can result in changes to arroyo stability (bank and head cutting) and sediment transport (Antevs, 1952; Schumm and Hadley, 1957; Bull, 1997; Waters and Haynes, 2001). Adjustment of channel slope or unit stream power can affect the longitudinal profile, cross section morphology, and incision of arroyo systems (Schumm and others, 1984; Homan, 2024). When the systems are combined with labile sediment (fine sand to silt), the available supply to the subbasins can greatly complicate the process of trying to trace the main driver of erosion (Gellis and others, 2005; Friedman and others, 2015).

Land-use change, historical rangeland grazing, and energy development can result in adjustment of channel form and stability and dominant erosive processes in arroyo systems (Lusby, 1979; Trimble and Mendel, 1995; Belsky and others, 1999; Entrekin and others, 2011; Fick and others, 2020). Roads, oil and gas pipelines, oil well pads, and other infrastructure are all surface disturbances that affect runoff, soil health, vegetation density, and the erodibility of sediments on the hillslopes and along crossings in fluvial areas (Williams and others, 2007; Entrekin and others, 2011). These types of land use can lead to soil compaction and loss of native plants (Al-Dousari and others, 2019), which can decrease precipitation infiltration and increase runoff (Greene and others, 1994). Surface disturbances also can damage biological crusts and increase soil erosion rates, making the area less tolerant to drought (Schwinning and others, 2008) and more prone to erosion during heavy precipitation (McAuliffe and others, 2006). Along with other methods, repeated surveys of arroyo cross sections in New Mexico (Leopold and others, 1966; Gellis and others, 2005; Friedman and others, 2015) showed some reaches began filling in the mid-1900s following the period of arroyo incision during late 1800s and early 1900s. Increasing development in a subbasin can affect aggradation and incision at different locations along arroyo channels, especially near road crossings (Gellis and others, 2005).

The four subbasins studied for this report represent headwater areas of the Stinking Water Creek Basin within a substrate of Mancos Shale. Although the subbasins are small secondary arroyos of the larger arroyo complex in the area (their entire area is only about 6 km^2 of the 112 km^2 basin; fig. 2), changes in these subbasins are accessible, relevant to energy development, have upper and lower terraces, and can be monitored through time. Although the subbasins examined in the study may not have experienced or recorded all of the regional wide erosion that could have taken place downstream and on the main stem of Stinking Water Creek where stream power is greater (Bull, 1997), statistical tests indicated differences between subbasins in terms of cross-section area, width, depth, and width-to-depth ratio which can be used to make inferences about regional arroyo incision.

The differences in channel morphology were not always aligned with land use (energy development subbasins compared to grazing-only subbasins). Generally, however, headwaters had smaller channel geometry (cross-section area) than downstream subbasins, which also had greater streamflow (table 1). Two terraces were studied in each subbasin; subbasin B2 differed from the other subbasins in several morphological characteristics for both terraces and also differed in other characteristics, as discussed in the following paragraphs.

Upper and lower terrace (fig. 4) cross-section area and width were greater in the downstream subbasins (A1 is 1.6 km^2 and B1 is 1.35 km^2) compared to the upstream subbasins (A2 is 1.5 km^2 and B2 is 1.6 km^2; figs. 7 and 8). The similarities between subbasins A1 and B1 (downstream subbasins) and A2 and B2 (upstream subbasins with higher elevations and steeper slopes) likely reflect their similar slopes and geographical proximity to the main stem of Stinking Water Creek (fig. 2). Photographs taken at the same headwater location in the Stinking Water Creek Basin in 1907 and 2019 (fig. 9) show little change to the landscape even after more than 100 years.

Cross-section depth and width-to-depth ratio differed between subbasins with separate land-use histories. For the upper and lower terrace datasets, median depths were smaller in the subbasins with energy development (A1 and A2) compared to the subbasins with rangeland grazing only (B1 and B2); subbasin B2 was the smallest (fig. 8). Median width-to-depth ratios were greatest in subbasin A1, followed by subbasins A2 and B1, and smallest in subbasin B2 (fig. 7), indicating channels in subbasins A1 and A2 are generally wider and shallower than channels in subbasins B1 and B2.

Comparison of channel morphology based on Q_{10} streamflows in the Stinking Water Creek subbasins shows differences between land-use histories with subbasins A1 and A2 having higher sinuosity, less shear stress, and greater width-to-depth ratios than cross sections in subbasins B1 and B2 (table 1). Along with the morphology differences discussed in the previous paragraph, this finding could indicate energy development in subbasins A1 and A2 may have caused channel evolution to progress from incision to widening processes, whereas subbasins B1 and B2 may still be incising. Stability may not yet be achieved in subbasins A1 and A2, and the widening process may be transporting sediment out of these subbasins. Subbasins A1 and A2 channels could have been narrower in the past but widened through time through processes such as soil piping or bank collapse. As discussed earlier, changes in arroyo systems can result from many factors, such as change in slope, flow regime (and thus vegetation) or high velocity flooding, (Antevs, 1952; Bull, 1997; Waters and Haynes, 2001) and observed differences between the subbasins might not be attributable to land use alone. The lower sinuosity and shear stress as well as higher width-to-depth ratios in subbasins A1 and B1 relative to subbasins A2 and B2 could indicate greater stability of cross sections in subbasins A1 and B1, which have lower slopes. Future development of energy resources could consider subbasin characteristics that can indicate greater stability to possibly reduce sediment transport and erosion, relative to subbasins showing instability before potential additional disturbances occur.

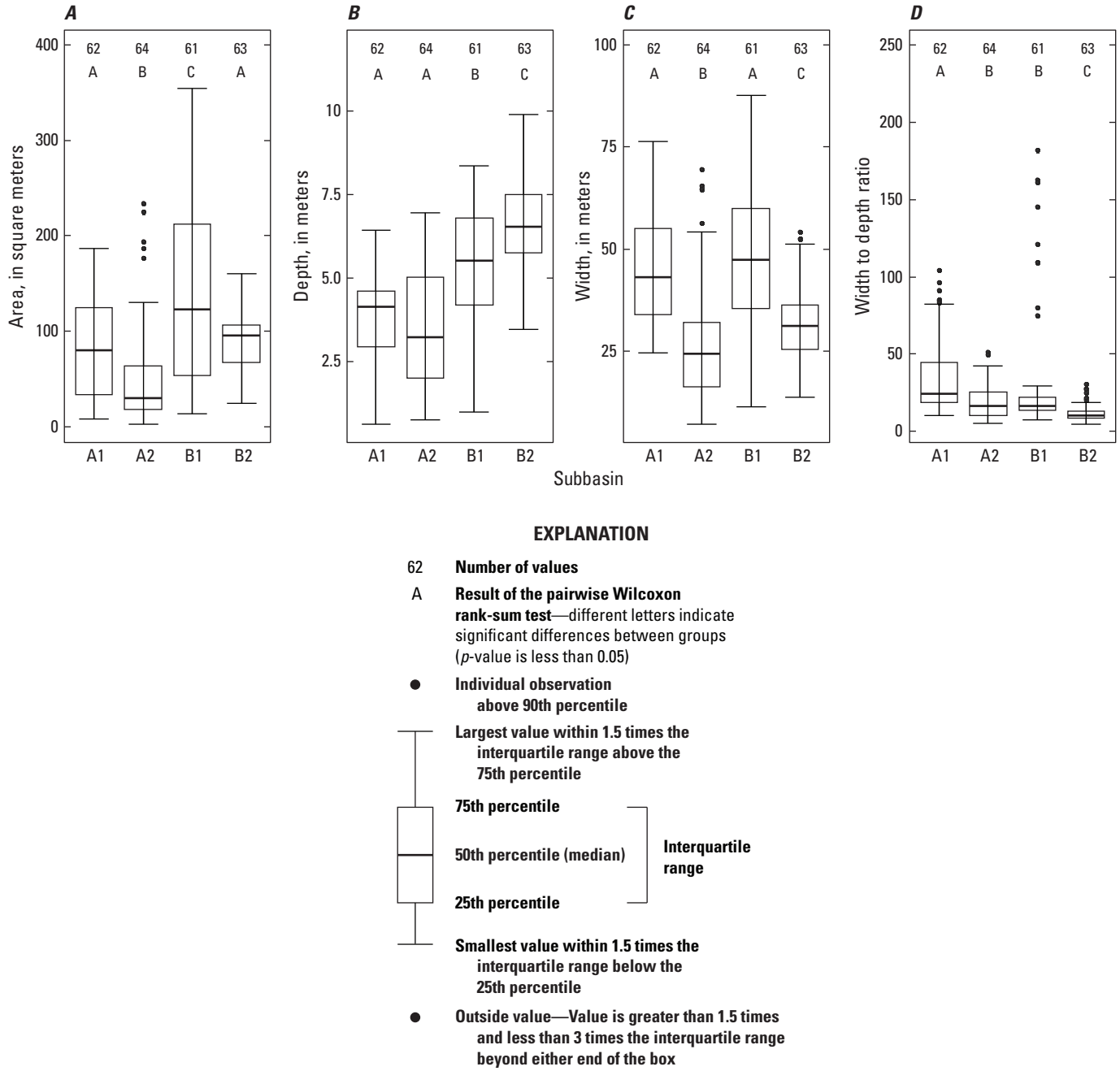


Figure 7. Summary of upper terrace to streambed cross-section *A*, area; *B*, depth; *C*, width; and *D*, width-to-depth ratio in the four subbasins. Letters within the plot area indicate significant differences between groups, as determined by the pairwise Wilcoxon rank-sum test. Data are available in Gidley and others (2026).

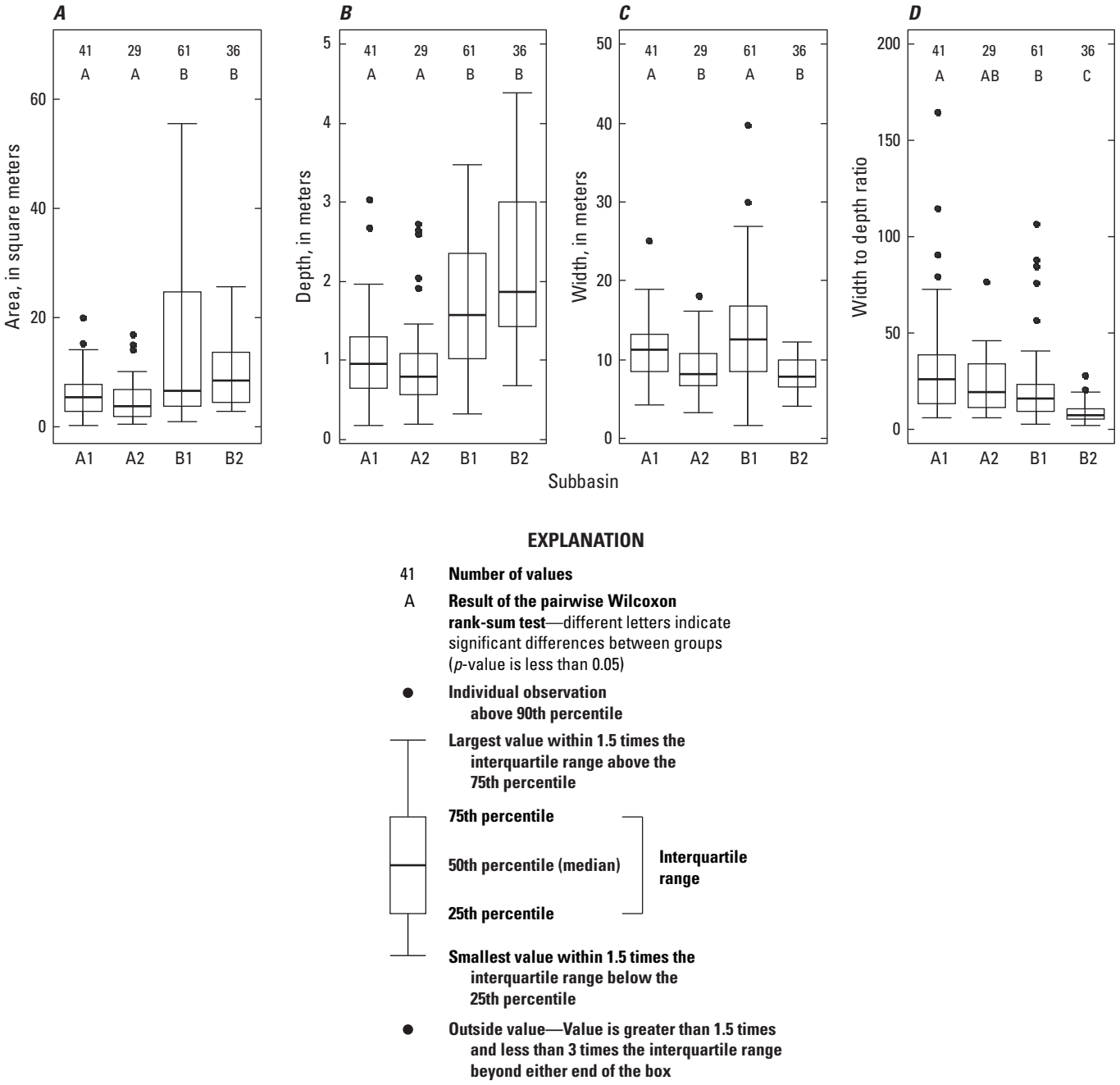


Figure 8. Summary of lower terrace to streambed cross-section *A*, area; *B*, depth; *C*, width; and *D*, width-to-depth ratio in the four subbasins. Letters within the plot area indicate significant differences between groups, as determined by the pairwise Wilcoxon rank-sum test. Data are available in Gidley and others (2026).

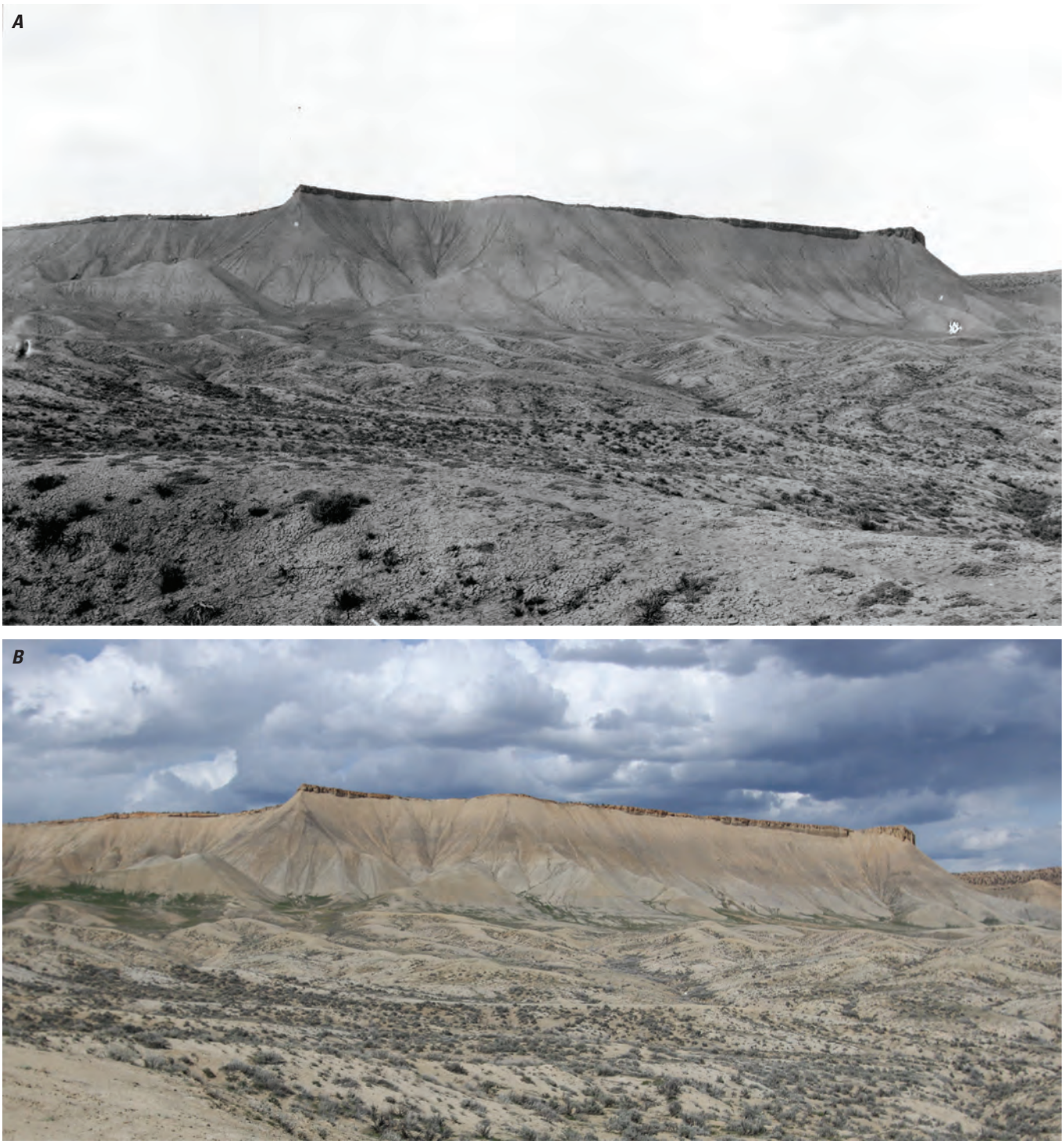


Figure 9. Photographs of landscape near Stinking Water Creek, near Rangely, Colorado, in *A*, 1907 (from Gale, 1908) and *B*, 2019 (photograph by Cory A. Williams, U.S. Geological Survey).

Luminescence Ages and Channel History

Sediment sample dating from the upper and lower terraces of each of the subbasins provided some insight into the past sediment transport. Samples collected at depth in the active channel were used to assess the age of alluvial materials beneath the active channel and indicated when the system was incising or aggrading. If the streambed age is old relative to the ages of terrace deposits, the stream is incising (cutting into and exposing the older alluvial fan surface). If the streambed age is young relative to the terrace deposits ages, the system is aggrading (depositing more material than it can carry away; Fischenich and others, 1989, Simon and Darby, 1997; Bledsoe, 1999).

There are several caveats to consider in the geomorphology of the four subbasins of Stinking Water Creek. An additional possibility could be the stream is incising into deposits that represent a period of recent aggrading conditions. But such complications would result in multiple stratigraphy age reversals, which this study's results did not support (table 5). Similarly, samples from the near surface of a terrace can also aid in a detailed assessment of when the active channel was last depositing sediments along those surfaces, but we did not attempt to precisely document mappable units in the local terraces. The relative thickness and depth of these deposits were not known because completing detailed surveys across the subbasins to correlate units was beyond the scope of the study.

There are also several caveats to keep in mind with OSL dating (refer to the Methods section of this report): (1) the ages determined for this study might be overestimated due to partial bleaching during turbulent, muddy, high flow; (2) because sediment was collected from one site in each subbasin, it is possible that better bleached sediments are present elsewhere in the subbasins; and (3) deposition could be inconsistent throughout the channels, with recent deposition occurring in areas other than the sampling sites as there could be multiple periods of incision intertwined with aggradation present in the subsurface. Upper terraces have older ages, lower terraces reflect younger ages, and the modern stream channel has the youngest OSL ages. However, if the stream is actively incising, then the modern stream channel has the oldest ages, because the stream is eroding or cutting into the older alluvial fan structure (Bull, 1990). Young sediment could mostly be depositing downstream and be found near the sink of the subbasins, which for this study is the White River, with older sediments left in various slackwater deposits further upstream within Stinking Water Creek.

The geologic map of the Rangely quadrangle (Cullins, 1971) shows Stinking Water Creek with a typical dendritic pattern of Quaternary alluvium (Qal) widely deposited in the small tributary subbasins (fig. 2) that is otherwise dominated by Mancos Shale. There are remnants of the lowest and youngest regional fill terrace (Quaternary terrace; Qt1) near the White River, but only one small outcrop is left near the study subbasins (at least 1 km south). Based on current (2026) knowledge, these regional fill terraces have never been dated, and this study was unable to establish access to an undeveloped Qt1 terrace for luminescence sampling during this study period. However, it is reasonable to presume this alluvium was deposited sometime after the Pinedale glaciation in the very eastern extent of the eastern Uinta Mountains of Utah and Colorado, because those mountains most likely source a large part of the alluvium now deposited within Stinking Water Creek Basin (Laabs and Munroe, 2018). This sediment could have mixed with the unconsolidated Mancos Shale at the surface to produce the Qal present today. Available sediment supply and much more precipitation than modern day could have facilitated the increased deposition of alluvium to build the smaller, local cut and fill terraces of Stinking Water Creek.

The smaller terraces of Stinking Water Creek have not been formally mapped but have been dated in four subbasins by OSL following the simplified scheme of the upper terrace, lower terrace, and streambed (figs. 4 and 10). Subbasins A1 and A2 are highly developed with oil and gas infrastructure whereas land use in subbasins B1 and B2 is ranchland grazing, such that subbasins B1 and B2 have significantly less disturbed land (table 10). These local cut and fill terraces are expected to be much younger than the larger, regional fill terraces established during glacial baseline change (Qt1, Qt2, and Qt3 of Cullins, 1971; older or close to 16,000–14,000 years; Laabs and Munroe, 2018).

In all four subbasins (A1, A2, B1, and B2), the upper terrace was dated at 960 ± 70 years (subbasin A1), 1,250 ± 220 years (subbasin A2), 970 ± 170 years (subbasin B1) and a substantially older 8,330 ± 770 years (subbasin B2; table 5; fig. 10). The most likely scenario is the depositional age of the terraces is an average of 960, 1,250, and 970 years. The 8,330 years likely reflect a partially bleached (residual signal not completely erased on transport) age that is not reliable or reflects different preservation of depositional layers in the cut and fill, and the terrace formation or reflects a different paced depositional rate due to land use. The age of the upper terrace was 985 ± 125 years, arriving at this as a weighted mean based on precision of the errors to each age.

The lower terrace was 910 ± 80 years (subbasin A1), 680 ± 70 years (subbasin A2), 730 ± 80 years (subbasin B1), and 2,000 ± 180 years (subbasin B2; fig. 10). Again, subbasin B2 has a much older age than the other three subbasins, so this study averaged 910, 680, and 730 years, and 2,000 years reflected a partially bleached age or varied thickness of cut and fill not found elsewhere. The age of the lower terrace was 765 ± 90 years (weighted mean).

The modern channel streambeds were sampled and have ages of 4,610 ± 440 years (subbasin A1), 3,110 ± 360 years (subbasin A2), 4,460 ± 640 years (subbasin B1) and 160 ± 10 years (subbasin B2; fig. 10). The age of the modern channel for subbasins A1, A2, and B1 was 3,830 ± 510 years, but subbasin B2 represents a special case as discussed in the next paragraph. The older age of the streambed relative to the terraces in subbasins A1, A2, and B1 could indicate the stream is incising into the alluvium and carrying the sediment out of the Stinking Water Creek system, downstream to the White River.

We propose two theories for the difference in terrace and modern channel ages observed in subbasin B2 compared to subbasins A1, A2, and B1. One possibility is that the very young age (160 ± 10 years) from the modern channel of subbasin B2 reflects a localized, preserved deposit from the most recent episode of aggradation rather than channel incision. In this scenario, this sample may represent sediment that escaped subsequent erosion, although lack of comparable evidence makes this interpretation difficult to confirm.. However, an equally compelling theory based on land use, disturbance (table 10), median sediment size (sandier in subbasin B2), placement in the Stinking Water Creek Basin (fig. 2), and differing luminescence ages of subbasin B2 (fig. 10), is the other subbasins are so highly disturbed (or were disturbed and then abandoned in more recent years) that evidence of regional incision around 150–170 years ago has been lost.

There could be an underlying reason the terraces are also older in subbasin B2 if we temporarily disregard the possibility of partial bleaching and simply masking what would otherwise be a uniform regional signal of aggradation. The upper terrace of subbasin B2 is much older than any other subbasin site (fig. 10) by a factor of 8.5. The lower terrace of subbasin B2 is also older but only by a factor of 2.5. The possibility of partial bleaching is a strong argument, because it is likely affected by the steeper gradients in subbasins A2 and B2 than in subbasins A1 and B1. Mean annual hillslope soil loss, channel soil loss, and sediment discharge from basin outlet were much greater in subbasins A1 and B1. However, partial bleaching cannot fully account for the observed pattern, because ages from subbasin A2 largely fell in line with subbasins A1 and B1. Potentially, this is because of the low disturbance rate of subbasin B2, and subbasins A1, A2, and B1 are responding to land disturbance by disparate movement of sediment in response to unknown local factors.

The highest terraces are older (Bull, 1990). The upper terrace was deposited between 860 and 1,110 calendar years ago (A.D. 1160 to 910 calculated from 2020), whereas the lower terrace was deposited between 675 and 855 calendar years ago (A.D. 1345 to 1165).During those periods, the system was aggrading. These ages are young enough that they cannot be the same age as the Qal beneath them, which are likely older than 16,000–14,000 years (Laabs and Munroe, 2018).

There is no record for any sediment between A.D. 1345 and A.D. 1860, because A.D. 1860 is the 160 ± 10-year-old age from subbasin B2. Although the subbasin B2 streambed sample represents the youngest age for sediments collected, it still predates the start of grazing and energy development in the area by a few decades unless there was undocumented grazing activity (1850–70 compared to the 1880s; fig. 5). Sometime 150–170 years ago, the system was gently aggrading, but not widely, and a preserved slice of that activity is observed in subbasin B2. Valley fills (or aggradation) have been found elsewhere, A.D. 1300–1880 (Harvey and others, 2011; Summa-Nelson and Rittenour, 2012; Townsend and others, 2019). Because there are no records of that time preserved in the samples from Stinking Water Creek, the inference is the system is generally incising, but the system is still aggrading in subbasin B2, which is bolstered by the substantially older ages of the upper and lower terraces when compared to subbasins A1, A2, and B1.

Post A.D. 1860, however, the system is actively incising, because the modern channel was found to be full of the alluvial sediment at deeper levels and at an older age, as expected if the stream was cutting into the older alluvium. No evidence of any sediment deposition or redeposition younger than 150 years was found, and results of this study concluded the system is incising in large enough floods that all material is being washed out of the subbasins and deposited close to the White River, which is the ultimate sink of the system. Determining whether the flow regime, flooding (frequency or intensity of rainfall), or land-use change was the primary driver for arroyo development would need further focused study.

Sediment Density and Chemistry

The median density of sediment samples collected along the main stem of Stinking Water Creek was 1.36 grams per cubic centimeter, which is within the typical range of densities for sandy, silty, and loamy soils (Natural Resources Conservation Service, 2019) and similar to bulk density values determined for alluvium derived from Mancos Shale sediment collected near Delta, Colorado (Tuttle and others, 2014; table 2).

Several studies have evaluated TDS or selenium in Mancos Shale sediment in western Colorado, providing comparison for the chemistry results of this study. TDS concentrations in the four Stinking Water Creek subbasins ranged from 360 mg/kg to 6,330 mg/kg, and subbasin B2 had lower concentrations compared to the other subbasins (table 3). Richards and others (2023) collected soil profiles at sediment-retention ponds near Delta, Colorado, and used water-sediment extraction similar to the process used for the Stinking Water Creek samples to measure TDS, resulting in concentrations between about 700 mg/kg and 85,550 mg/kg (Richards, 2022). Within the soil profiles, TDS concentrations were lower near the surface and higher at depth (Richards and others, 2023).

Selenium concentrations for the Stinking Water Creek samples were between 0.10 µg/g and 0.36 µg/g (table 4). The highest value came from the upper terrace of subbasin A2 and the lowest value came from the lower terrace of subbasin A2. The mean and median of subbasin A2 fell within the range of subbasins A1 and B1, and only subbasin B2 standing out with an overall higher concentration in every terrace (0.31 µg/g in the upper terrace, 0.33 µg/g in the lower terrace, and 0.28 µg/g in the streambed; table 4). Because subbasin B2 is less disturbed and also the most incised (as opposed to widening) subbasin studied (figs. 5, 7, and 8), the higher selenium values in subbasin B2 could be from the Mancos Shale not redeposited, mixed, or otherwise converted to Qal. Several other studies of selenium in sediment from Mancos Shale in western Colorado have found total selenium concentrations ranging from about 0.3 to 33.3 µg/g (Tuttle and others, 2014; Mills and others,

2016; Elrashidi, 2017). Selenium concentrations increase with depth, because selenium at the surface can be moved by runoff or irrigation water (Tuttle and others, 2014; Elrashidi, 2017). Mills and others (2016) compared selenium concentrations in cores of Mancos Shale to alluvium formed from weathered Mancos Shale and found lower concentrations in the alluvium.

Sediment, Salinity, and Selenium Loads

The sediment, salinity, and selenium load estimates presented in this report are provided as snapshots representing concentrations at a single point in time. These values are not actual loads related to erosion or concentrations in the past but calculations based on the small dataset of this study. Basin characteristics such as topography and land use were important factors in WEPP simulations. Calculated mean annual hillslope soil loss, channel soil loss, and sediment discharge from basin outlet were much greater in subbasins A2 and B2, which have steeper gradients than subbasins A1 and B1 (table 7). Differences between land use were apparent in the results of WEPP:Road simulations. Due to more extensive infrastructure associated with energy development (fig. 3), subbasins A1 and A2 have more road-related sediment loss than subbasins B1 and B2 (table 7). Despite the longer road length in subbasin A1, amounts of sediment leaving the roads and buffers were larger for subbasin A2, which could reflect the increased traffic and wider roads in subbasin A2 compared with subbasin A1 (fig. 3).

Incision rates were calculated using the change in channel volume between OSL ages determined for the geomorphic surfaces (when the sediments were deposited). Actual incision rates were likely not constant throughout time but are provided to compare potential sediment storage and transfer dynamics in the subbasins. Estimated sediment, salinity, and selenium loads (tables 4 and 8) were generally greater in the downstream subbasins (A1 and B1) compared to the upstream subbasins (A2 and B2). As discussed previously, channels in the downstream subbasins, particularly subbasin B1, have larger cross-section areas than the upstream subbasins. Due to their size, incision in these larger channels can lead to greater volume change and therefore more sediment. This increase in cross-sectional area could also be a result of longer exposure to erosional processes. The energy required to drive erosional processes may not occur until lower in the subbasins, and changes in slope lower in the subbasin could also spread energy across a broader area, resulting in wider channel formation.

Subbasin B2 generally had smaller sediment, salinity, and selenium annual loads than the other subbasins (tables 8 and 9). Subbasin B2 also had unusual luminescence ages not aligned with the other three subbasins and indicated preserved aggradation as recently as 150–170 years ago. The geology of subbasin B2 has more sandstone than the other subbasins (fig. 2) and is on the east side of the main stem Stinking Water Creek (the other three subbasins are on the western side of the main stem), which might contribute to the differences in OSL ages and erosional history.

Potential Additional Geochronology Studies

The calculations presented in this report rely on a small dataset of OSL ages that greatly affect the incision rate and load calculations. For example, although subbasins A1 and B2 had similar change in channel volume, differences in the OSL ages indicate subbasin A1 has a much higher incision rate (table 8). The OSL ages in subbasins A1, A2, and B1 are closely aligned, but the age of the upper terrace in subbasin B2 was much older than the terrace ages in the other subbasins (table 5), and the age of lower terrace was somewhat older than the other subbasins. The difference in OSL ages in subbasin B2 could be related to differing erosional processes of land use, geology, or the subbasin's location on the eastern side of Stinking Water Creek. These differences potentially could be explored with additional study.

The depth and location of OSL samples can greatly affect the resulting age; the accompanying incision rates and load estimates potentially could therefore be refined by additional OSL dating within the Stinking Water Creek Basin with additional data points on the eastern side of the main stem. Because headwater areas may not show channel effects present downstream (Bull, 1997), potential additional dating of terrace surfaces further downstream on the main stem of Stinking Water Creek and at the confluence with the White River could identify additional luminescence field locations, provide more information about historical channel position and the effects of land-use practices, improve the understanding of channel history, and provide detail for measuring incision rates and sediment, salinity, and selenium loads.

Other dating techniques potentially could also be used to supplement and support OSL dating. Radiocarbon dating of organic material, such as charcoal, can help to constrain luminescence deposition of sediment ages (Harvey and others, 2011; Summa-Nelson and Rittenour, 2012; Townsend and others, 2019). Similarly, radioisotope dating with cesium-137 and lead-210 potentially can be used to date recent deposits (after 1950; Harvey and others, 2011; Poreba and others, 2015) to test the hypothesis that incision has been the dominant stream mode for at least 50 years or more. Portable OSL readers produce relative luminescence signals for sediments rather than absolute ages (that is, full OSL analysis) and potentially can be a useful tool for site reconnaissance and screening. Portable OSL analysis is less expensive and time consuming than full OSL analysis (Munyikwa and others, 2020), making it possible to potentially analyze many samples and pinpoint the layers of stratigraphy with the best bleached grains whether these may be from the cut or fill layers. This study hypothesizes that the cut layers will be younger than the fill layers due to transport during sunlight exposure during the flood or flow. Potential additional work in Stinking Water Creek could benefit from use of portable OSL to investigate a multitude of possible potential sampling locations in a rapid fashion and pinpoint where full OSL sampling and measurement could be most beneficial.

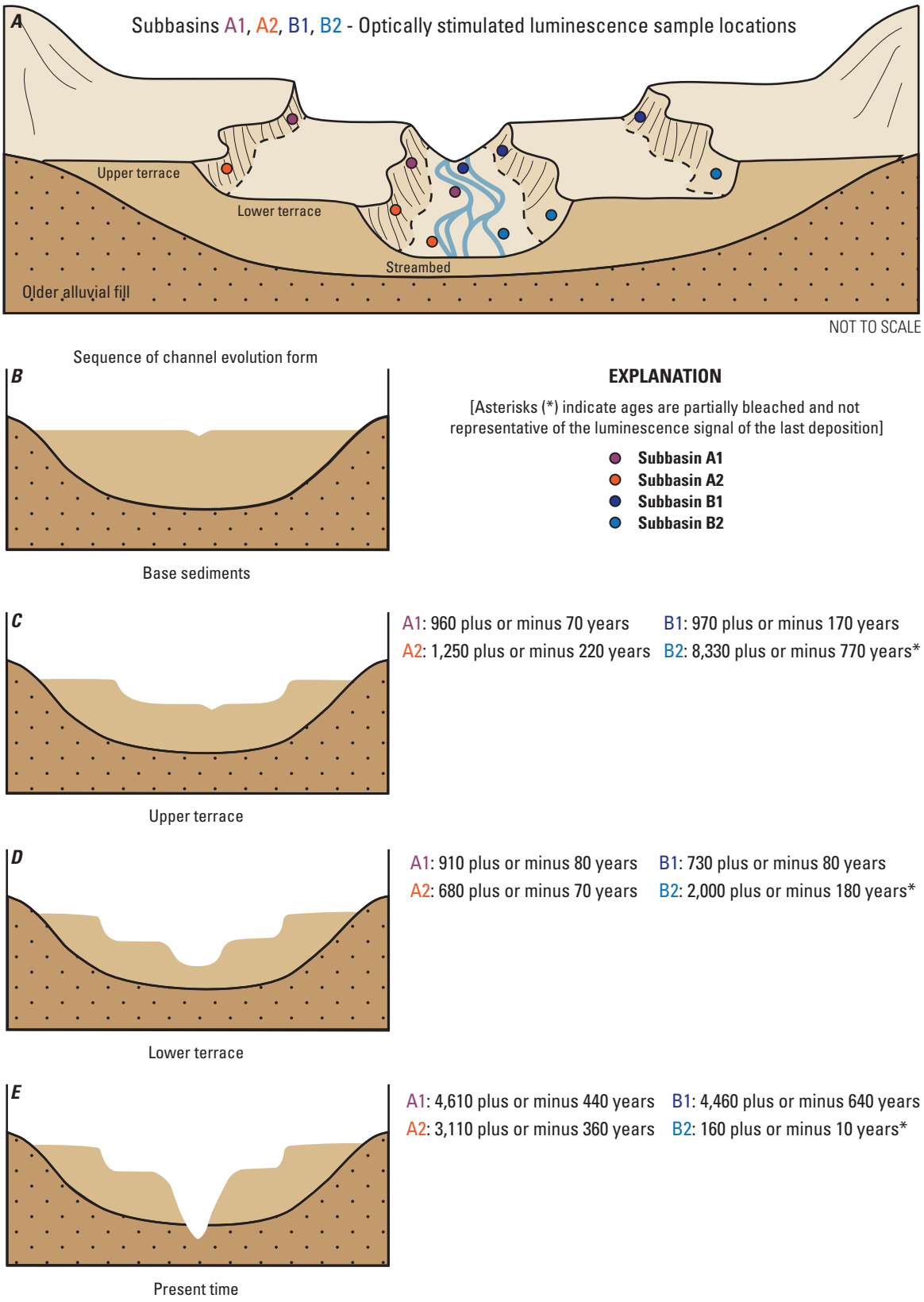


Figure 10. *A–E*, Potential channel history determined from optically stimulated luminescence dating in the four subbasins (A1, A2, B1, and B1), which are local terraces to the main stem of Stinking Water Creek, near Rangely Colorado.

Summary

This report provides a characterization for a timeline of land-use change in four subbasins of Stinking Water Creek near Rangely, Colorado. Stinking Water Creek is floored in Mancos Shale, which is a source of sediment, salinity, and selenium to surface water in many areas of western Colorado. Natural and human activity disturbances to the alluvium and Mancos Shale expose and move these constituents. Understanding if and how some common land uses affect channel storage and delivery of these constituents has important implications for management decisions.

The U.S. Geological Survey, in cooperation with the Bureau of Land Management, studied terrace surfaces in four subbasins of Stinking Water Creek. Rangeland grazing is present in all four subbasins, and two subbasins have energy (oil and gas) infrastructure (subbasins A1 and A2) and the other two subbasins do not (subbasins B1 and B2). Subbasins A1 and B1 are downstream relative to subbasins A2 and B2, which means A2 and B2 have higher elevation and steeper slopes. Aerial photographs, sediment chemistry, optically stimulated luminescence (OSL) ages, cross-section surveys, and Watershed Erosion Prediction Project modeling were used to characterize the history of land-use change by estimating stream channel incision rates, sediment transport, and salinity and selenium loads.

Channel cross-section area, width, depth, and width-to-depth ratio differed between the four subbasins; however, the differences were not always related land use but to the subbasin position (upstream compared to downstream). Upper and lower terrace cross-section area and width were greater in the downstream subbasins (A1 and B1) compared to the upstream subbasins (A2 and B2). Generally, headwater areas have smaller channels than downstream subbasins with greater streamflow, and the similarities between subbasins likely reflect their similar geographic settings with respect to Stinking Water Creek.

Upper and lower terrace median depths were smaller in the subbasins with energy development (subbasins A1 and A2) when compared to the subbasins with rangeland grazing only (subbasins B1 and B2). Median width-to-depth ratios were greatest in subbasin A1, followed by subbasins A2 and B1, and smallest in subbasin B2. Subbasins A1 and A2 also had higher sinuosity and less shear stress. Channels in subbasins A1 and A2 were generally wider and shallower than channels in subbasins B1 and B2. Landscape disturbances related to energy development in subbasins A1 and A2 could have caused channel evolution to progress from incision to widening processes, whereas subbasins B1 and B2 could still be incising.

All subbasins had an upper and lower terrace and a modern streambed channel. Using OSL dating on the sediment of the terraces and streambed channel, the age of the upper terrace was placed at 985 ± 125 years, leaving out subbasin B2 as its age was 8 times older than the other subbasins. The weighted mean age of the lower terrace was 765 ± 90 years, again leaving out subbasin B2, because its age was 2 times older than the other subbasins. The age of the modern channel in subbasins A1, A2, and B1 was 3,830 ± 510 years, but the stream channel in subbasin B2 was much younger 160 ± 10 years. The study results found that in subbasins A1, A2, and B1, the streambed age was older than the terraces, indicating the channels are incising and widening into the older alluvium.

There are two theories hypothesized for why the young age of the subbasin B2 streambed was not found elsewhere. The first theory is that the sampled material represents the last time this stretch was aggrading and not incising. The second theory—based on the land use, disturbance, median sediment size (sandier in subbasin B2), placement in the Stinking Water Creek Basin, and differing luminescence ages of subbasin B2—is that the other subbasins are so highly disturbed (or were disturbed and then abandoned in more recent years) that evidence of regional incision around 150–170 years ago has been lost in the other subbasins.

Prior to A.D. 1870, the system likely alternated between largely aggradation and smaller occurrences of incision, after 1870, however, the system is dominantly incising in subbasins A1, A2, and B1, because the modern channel was found to be full of the alluvial sediment at deeper levels and an older age, as expected if the stream was cutting into the older alluvium. The older terrace ages and young streambed age in subbasin B2 supports aggradation as the main process in this subbasin unlike the other three. Determination of whether flow regime, flooding (frequency or intensity of rainfall), or land-use change was the primary driver for arroyo development is not possible without potential further focused study.

Watershed Erosion Prediction Project modeling results in combination with changes in channel volume were used to predict sediment, salinity, and selenium loads. The load values are estimates representing concentrations at one point in time and are provided to compare potential sediment storage and transfer dynamics in the subbasins. Loads were generally greater in the downstream subbasins (A1 and B1) compared to the upstream subbasins (A2 and B2). Although subbasins A1 and A2 had significant sediment loss from road buffers, subbasin B1 had the greatest sediment, salinity, and selenium loads, likely due to large cross-section areas and therefore large volume change. Subbasin B2 generally had smaller sediment, salinity, and selenium annual loads than the other subbasins, likely due to the small cross-section area and the long time period used to estimate loads.

References Cited

Aby, S., 2017, Date of arroyo cutting in the American Southwest and the influence of human activities: Anthropocene, v. 18, p. 76–88, accessed July 13, 2020, at https://doi.org/10.1016/j.ancene.2017.05.005.

Al-Dousari, A.M., Alsaleh, A., Ahmed, M., Misak, R., Al-Dousari, N., Al-Shatti, F., Elrawi, M., and William, T., 2019, Off-road vehicle tracks and grazing points in relation to soil compaction and land degradation: Earth Systems and Environment, v. 3, p. 471–482, accessed October 2021 at https://doi.org/10.1007/s41748-019-00115-y.

Antevs, E., 1952, Arroyo-cutting and filling: The Journal of Geology, v. 60, no. 4, p. 375–385, accessed August 20, 2020, at https://doi.org/10.1086/625985.

Beck, H.E., Zimmerman, N.E., McVicar, T.R., Vergopolan, N., Berg, A., and Wood, E.F., 2018, Present and future Köppen-Geiger climate classification maps at 1-km resolution: Scientific Data, v. 5, article no. 180214, 12 p., accessed June 9, 2023, at https://doi.org/10.1038/sdata.2018.214.

Belnap, J., Reynolds, R.L., Reheis, M.C., Phillips, S.L., Urban, F.E., and Goldstein, H.L., 2009, Sediment losses and gains across a gradient of livestock grazing and plant invasion in a cool, semi-arid grassland, Colorado Plateau, U.S.A.: Aeolian Research, v. 1, no. 1–2, p. 27–43, accessed December 6, 2021, at https://doi.org/10.1016/j.aeolia.2009.03.001.

Belsky, A.J., Matzke, A., and Uselman, S., 1999, Survey of livestock influences on stream and riparian ecosystems in the western United States: Journal of Soil and Water Conservation, v. 54, no. 1, p. 419–431, accessed December 12, 2023, at https://doi.org/10.1080/00224561.1999.12457258.

Benjamini, Y., and Hochberg, Y., 1995, Controlling the false discovery rate—A practical and powerful approach to multiple testing: Journal of the Royal Statistical Society—Series B (Methodological), v. 57, no. 1, p. 289–300, accessed March 17, 2022, at https://doi.org/10.1111/j.2517-6161.1995.tb02031.x.

Bern, C.R., Clark, M.L., Schmidt, T.S., Holloway, J.M., and McDougal, R.R., 2015, Soil disturbance as a driver of increased stream salinity in a semiarid watershed undergoing energy development: Journal of Hydrology, v. 524, p. 123–136, accessed December 14, 2021, at https://doi.org/10.1016/j.jhydrol.2015.02.020.

Bern, C.R., Williams, C.A., and Smith, C.G., 2023, Source contributions to suspended sediment and particulate selenium export from the Loutsenhizer Arroyo and Sunflower Drain watersheds in Colorado: U.S. Geological Survey Scientific Investigations Report 2023–5056, 32 p., accessed June 5, 2023, at https://doi.org/10.3133/sir20235056.

Bledsoe, B.P., 1999, Specific stream power as an indicator of channel pattern, stability, and response to urbanization: Fort Collins, Colorado, Colorado State University, Ph.D. dissertation, p. 1–24.

Briggs, P.H., and Crock, J.G., 1986, Automated determination of total selenium in rocks, soils, and plants: U.S. Geological Survey Open-File Report 86–40, 20 p, accessed December 9, 2020, at https://doi.org/10.3133/ofr8640.]

Bryan, R.B., and Jones, J.A.A., 1997, The significance of soil piping processes—Inventory and prospect: Geomorphology, v. 20, p. 209–218, accessed May 24, 2022, at https://doi.org/10.1016/S0169-555X(97)00024-X.

Bull, W.B., 1990, Stream-terrace genesis—Implications for soil development: Geomorphology, v. 3, no., 3–4, p. 351–367, accessed August 19, 2025, at https://doi.org/10.1016/0169-555X(90)90011-E.

Bull, W.B., 1997, Discontinuous ephemeral streams: Geomorphology, v. 19, no. 3–4, p. 227–276, accessed July 13, 2020, at https://doi.org/10.1016/S0169-555X(97)00016-0.

Bureau of Reclamation, 2005, Quality of water—Colorado River Basin Progress Report no. 22: Bureau of Reclamation, 69 p., accessed June 12, 2023, at https://www.usbr.gov/uc/progact/salinity/pdfs/PR22.pdf.

Bureau of Reclamation, 2019, Quality of water Colorado River Basin—Progress report no. 26: Bureau of Reclamation, 130 p., accessed June 12, 2023, at https://www.usbr.gov/uc/progact/salinity/pdfs/ProgressReports/20190000-QualityWaterColoradoRiverBasin-ProgressReport26-508-UCRO.pdf.

Butler, D.L., 1996, Trend analysis of selected water-quality data associated with salinity-control projects in the Grand Valley, in the lower Gunnison River Basin, and at Meeker Dome, western Colorado: U.S. Geological Survey Water-Resources Investigations Report 95–4274, 38 p., accessed December 8, 2021, at https://doi.org/10.3133/wri954274.

Butler, D.L., 2001, Effects of piping irrigation laterals on selenium and salt loads, Montrose Arroyo Basin, western Colorado: U.S. Geological Survey Water-Resources Investigations Report 2001–4204, 14 p., accessed December 8, 2021, at https://doi.org/10.3133/wri014204.

Butler, D.L., Krueger, R.P., Osmundson, B.C., Thompson, A.L., and McCall, S.K., 1991, Reconnaissance investigation of water quality, bottom sediment, and biota associated with irrigation drainage in the Gunnison and Uncompahgre River basins and at Sweitzer Lake, west-central Colorado, 1988–89: U.S. Geological Survey Water-Resources Investigations Report 91–4103, 107 p.

Butler, D.L., Wright, W.G., Hahn, D.A., Krueger, R.P., and Osmundson, B.C., 1994, Physical, chemical, and biological data for detailed study of irrigation drainage in the Uncompahgre Project area and in the Grand Valley, west-central Colorado, 1991–92: U.S. Geological Survey Open File Report 94–110, 146 p., accessed November 7, 2022, at https://doi.org/10.3133/ofr94110.

Butler, D.L., Wright, W.G., Steward, K.G., Campbell Osmundson, B., Krueger, R.P., and Crabtree, D.W., 1996, Detailed study of selenium and other constituents in water, bottom sediment, soil, alfalfa, and biota associated with irrigation drainage in the Uncompahgre project area and in the Grand Valley, west-central Colorado, 1991–93: U.S. Geological Survey Water-Resources Investigations Report 96–4138, 136 p. [Also available at https://pubs.usgs.gov/wri/1996/4138/report.pdf.]

Buylaert, J., Huot, S., Murray, A.S., and Van Den Haute, P., 2011, Infrared stimulated luminescence dating of an Eemian (MIS 5e) site in Denmark using K-feldspar: Boreas, v. 40, no. 1, p. 46–56, accessed February 23, 2022, at https://doi.org/10.1111/j.1502-3885.2010.00156.x.

Chapman, P.M., Adam, W.J., Brooks, M.L., Delos, C.G., Luoma, S.N., Maher, W.A., Ohlendorf, H.M., Presser, T.S., and Shaw, D.P., eds., 2010, Ecological assessment of selenium in the aquatic environment: Boca Raton, Florida, CRC Press, 368 p. [Also available at https://doi.org/10.1201/EBK1439826775.]

Colorado Geological Survey, 2005, OF-05-09 shapefiles of the oil and gas fields map of Colorado: Colorado Geological Survey web page, open file report 05–09, accessed December 20, 2021, at https://coloradogeologicalsurvey.org/publications/shapefiles-oil-gas-fields-map-colorado.

Colorado River Basin Salinity Control Forum, 2017, Welcome to the Colorado River Basin Salinity Control Forum website: Colorado River Basin Salinity Control Forum web page, accessed September 13, 2017, at https://coloradoriversalinity.org/

Colorado School of Mines, 2005, ChevronTexaco's Rangely oil field operations: Energy and Minerals Field Institute field-program handout, accessed on September 20, 2017, at https://web.archive.org/web/20160108201522/http://emfi.mines.edu/emfi2005/ChevronTexaco.pdf.

Conley, J.M., Funk, D.H., Hesterberg, D.H., Hsu, L.-C., Kan, J., Liu, Y.-T., and Buchwalter, D.B., 2013, Bioconcentration and biotransformation of selenite versus selenate exposed periphyton and subsequent toxicity to the mayfly *Centroptilum triangulifer*: Environmental Science & Technology, v. 47, no. 14, p. 7965–7973, accessed May 13, 2021, at https://doi.org/10.1021/es400643x.

Cullins, H.L., 1971, Geologic map of the Rangely quadrangle, Rio Blanco County, Colorado: U.S. Geological Survey Quadrangle 903, 1 map, map scale 1:24,000, accessed April 2025 at https://doi.org/10.3133/gq903.

Daly, C., Halbleib, M., Smith, J.I., Gibson, W.P., Doggett, M.K., Taylor, G.H., Curtis, J., and Pasteris, P.P., 2008, Physiographically sensitive mapping of climatological temperature and precipitation across the conterminous United States: International Journal of Climatology, v. 28, no. 15, p. 2031–2064. [Also available at https://doi.org/10.1002/joc.1688.]

Day, N.K., Preston, T.M., and Longley, P.C., 2024, Wildland fire effects on sediment, salinity, and selenium yields in a basin underlain by Cretaceous marine shales near Rangely, Colorado: U.S. Geological Survey Scientific Investigations Report 2024–5043, 31 p., accessed December 10, 2025, at https://doi.org/10.3133/sir20245043.

Dean, J.R., 2005, Practical inductively coupled plasma spectroscopy: West Sussex, England, John Wiley & Sons, Ltd., 208 p. [Also available at https://doi.org/10.1002/047009351X.]

deBruyn, A.M.H., and Chapman, P.M., 2007, Selenium toxicity to invertebrates—Will proposed thresholds for toxicity to fish and birds also protect their prey?: Environmental Science & Technology, v. 41, no. 5, p. 1766–1770, accessed May 13, 2021, at https://doi.org/10.1021/es062253j.

Dewitz, J., 2019, National Land Cover Database 2016 products (ver. 3.0, November 2023): U.S. Geological Survey data release, accessed May 11, 2026, at https://doi.org/10.5066/P96HHBIE.

Elliot, W.J., 2004, WEPP internet interfaces for forest erosion prediction: Journal of the American Water Resources Association, paper no. 02021, p. 299–309, accessed January 13, 2022, at https://forest.moscowfsl.wsu.edu/engr/library/Elliot/Elliot2004k/2004k.pdf.

Elliott, J.G., Herring, J.R., Ingersoll, G.P., Kosovich, J.J., and Fahy, J., 2008, Rainfall-runoff and erosion data from the Mancos Shale Formation in the Gunnison Gorge National Conservation Area, southwestern Colorado, 2003–2006: U.S. Geological Survey Open-File Report 2007–1002G, 67 p. [Also available at https://pubs.usgs.gov/of/2007/1002/G/.]

Elliot, W., 2021, WEPP—road: U.S. Department of Agriculture Forest Service web page, accessed January 4, 2022, at https://web.archive.org/web/20160108201522/http://emfi.mines.edu/emfi2005/ChevronTexaco.pdf.

Elrashidi, M.A., 2017, Selenium distribution for soils derived from Mancos Shale in Gunnison and Umcompahgre River Basins, west-central Colorado: Communications in Soil Science and Plant Analysis: vol. 49, no. 9, p. 1083–1091, accessed January 2026 at https://doi.org/10.1080/00103624.2018.1448858.

Entrekin, S., Evans-White, M., Johnson, B., and Hagenbuch, E., 2011, Rapid expansion of natural gas development poses a threat to surface waters: Frontiers in Ecology and the Environment, v. 9, no. 9, p. 503–511, accessed June 24, 2022, at https://doi.org/10.1890/110053.

Esri, 2015, ArcMap: Redlands, Calif., Environmental Systems Research Institute, ver. 10.3.1.

Esri, 2020, ArcMap: Redlands, Calif., Environmental Systems Research Institute, ver. 10.8.1.

Fick, S.E., Belnap, J., and Duniway, M.C., 2020, Grazing-induced changes to biological soil crust cover mediate hillslope erosion in long-term exclosure experiment: Rangeland Ecology & Management, v. 73, no. 1, p. 61–72, accessed October 2021 at https://doi.org/10.1016/j.rama.2019.08.007.

Fischenich, J.C., Woessmer, W., and Potts, D.F., 1989, Channel erosion analysis and control, symposium proceedings: Headwaters Hydrology, American Water Resources Association.

Fishman, M.J., and Friedman, L.C., eds., 1989, Methods of determination of inorganic substances in water and fluvial sediments (3d ed.): U.S. Geological Survey Techniques of Water-Resources Investigations 05–A1, 545 p., accessed June 22, 2020, at https://doi.org/10.3133/twri05A1.

Flanagan, D.C., Frankenberger, J.R., Cochrane, T.A., Renschler, C.S., and Elliott, W.J., 2013, Geospatial application of the Water Erosion Prediction Project (WEPP) model: Transactions of the American Society of Agricultural and Biological Engineers, v. 56, no. 2, p. 591–601, accessed January 13, 2022, at https://www.fs.usda.gov/rm/pubs_other/rmrs_2013_flanagan_d001.pdf.

Flanagan, D.C., and Livingston, S.J., eds., 1995, WEPP user summary: West Lafayette, Indiana, U.S. Department of Agriculture, National Soil Erosion Research Laboratory Report No. 11, 131 p., accessed December 2022 at https://www.ars.usda.gov/ARSUserFiles/50201000/WEPP/usersum.pdf.

Flanagan, D.C., and Nearing, M.A., eds., 1995, USDA—Water Erosion Prediction Project hillslope profile and watershed model documentation: U.S. Department of Agriculture, National Soil Erosion Research Laboratory Report No. 10., variously paged, accessed December 2022 at https://www.ars.usda.gov/midwest-area/west-lafayette-in/national-soil-erosion-research/docs/wepp/wepp-model-documentation/

Friedman, J.M., Vincent, K.R., Griffin, E.R., Scott, M.L. Shafroth, P.B., and Auble, G.T., 2015, Processes of arroyo filling in northern New Mexico, U.S.A.: GSA Bulletin, v. 127, no. 3–4, p. 621–640, accessed December 2022 at https://doi.org/10.1130/B31046.1.

Gale, H.S., 1908, Geology of the Rangely oil district, Rio Blanco County, Colorado, with a section on the water supply: U.S. Geological Survey Bulletin 350, 61 p., accessed December 9, 2020, at https://doi.org/10.3133/b350.

Garbrecht, J., and Martz, L.W., 1997, TOPAZ—An automated digital landscape analysis tool for topographic evaluation, drainage identification, watershed segmentation, and subcatchment parameterization—Overview: U.S. Department of Agriculture, USDA-ARS-NAWQL 95-1.

Gellis, A.C., Emmett, W.W., and Leopold, L.B., 2005, Channel and hillslope processes revisited in the Arroyo de los Frijoles near Santa Fe, New Mexico: U.S. Geological Survey Professional Paper 1704, 53 p., accessed February 2022 at https://doi.org/10.3133/pp1704.

Gidley, R.G., Williams, C.A., Stevens, M.R., Kohn, M.S., and Homan, J.W., 2026, Landscape alteration, sediment chemistry, cross section, sediment transport, and load data for Stinking Water Creek, Rio Blanco County, Colorado, 2015–20: U.S. Geological Survey data release, https://doi.org/10.5066/P9R3YPO1.

Graham, J., 2015, Investigation into the timing of downcutting, Douglas Creek arroyo, Rangely, Rio Blanco County, Colorado [abs.]—Rocky Mountain Section, 67th Annual Meeting, Colorado Mesa University, Grand Junction, Colo., May 21–23: Geological Society of America Abstracts with Programs, v. 47, no. 6, p. 5, accessed December 12, 2023, at https://gsa.confex.com/gsa/2015RM/webprogram/Paper255956.html.

Greene, R.S.B., Kinnell, P.I.A., and Wood, J.T., 1994, Role of plant cover and stock trampling on runoff and soil erosion from semi-arid wooded rangelands: Soil Research, v. 32, no. 5, p. 953–973, accessed August 25, 2025, at https://doi.org/10.1071/SR9940953.]

Griffin, E.R., and Friedman, J.M., 2015, Processes limiting depth of arroyo incision—Examples from Rio Puerco, New Mexico, *in* Proceedings of the 5th Federal Interagency Hydrologic Modeling Conference and the 10th Federal Interagency Sedimentation Conference, Reno, Nevada, April 19–23, 2015: ACWI Subcommittee on Sedimentation and Subcommittee on Hydrology, p. 797–808.

Hamilton, S.J., 1998, Selenium effects on endangered fish in the Colorado River Basin, *in* Frankenberger W.T., and Engderg, R.A., eds., Environmental chemistry of selenium: New York, N.Y., Marcel Dekker, Inc., 713 p.

Harvey, J.E., Pederson, J.L., and Rittenour, T.M., 2011, Exploring relations between arroyo cycles and canyon paleoflood records in Buckskin Wash, Utah—Reconciling scientific paradigms: GSA Bulletin, v. 123, no. 11–12, p. 2266–2276, accessed May 2021 at https://doi.org/10.1130/B30374.1.

Hayden, F.V., 1878, Tenth annual report of the United States geological and geographical survey of the territories, embracing Colorado and parts of adjacent territories, being a report of progress of the exploration for the year 1876: U.S. Geological Survey annual report, 546 p., accessed August 25, 2025, at https://doi.org/10.3133/70038934.

Hayden, A., 2008, Douglas Creek revisited—Evidence for climate-driven arroyo incision in western Colorado [abs.]—2008 joint meeting between The Geological Society of America, Soil Science Society of America, American Society of Agronomy, Crop Science Society of America, Gulf Coast Association of Geological Societies with the Gulf Coast Section of SEPM, and the Houston Geological Society, Houston, Texas, October 5–9: Geological Society of America Abstracts with Programs, v. 40, no. 6, p. 464, accessed September 12, 2023, at https://gsa.confex.com/gsa/2008AM/webprogram/Paper150991.html.

Hawkins, S.J., Charpentier, R.R., Schenk, C.J., Leathers-Miller, H.M., Klett, T.R., Brownfield, M.E., Finn, T.M., Gaswirth, S.B., Marra, K.R., Le, P.A., Mercier, T.J., Pitman, J.K., and Tennyson, M.E., 2016, Assessment of continuous (unconventional) oil and gas resources in the Late Cretaceous Mancos Shale of the Piceance Basin, Uinta-Piceance Province, Colorado and Utah, 2016: U.S. Geological Survey Fact Sheet 2016–3030, 4 p., accessed December 9, 2020, at https://doi.org/10.3133/fs20163030.

Hayden-Lesmeister, A., and Rittenour, T.M., 2014, Chronostratigraphy of Holocene valley-fill alluvium and arroyo cut-fill events in the Upper Escalante River, southern Utah, *in* MacLean, J.S., Biek, R.F., and Huntoon, J.E., eds., Geology of Utah's far south: Utah Geological Association Publication 43, p. 57–76.

Helsel, D.R., Hirsch, R.M., Ryberg, K.R., Archfield, S.A., and Gilroy, E.J., 2020, Statistical methods in water resources: U.S. Geological Survey Techniques and Methods, book 4, chap. A3, 458 p., accessed March 17, 2022, at https://doi.org/10.3133/tm4a3. [Supersedes USGS Techniques of Water-Resources Investigations, book 4, chap. A3, version 1.1.]

Henry, B.L., and Wesner, J.S., 2018, Severing ties—Different responses of larval and adult aquatic insects to atrazine and selenium: Environmental Science & Technology, v. 52, no. 15, p. 8848–8857, accessed May 13, 2021, at https://doi.org/10.1021/acs.est.8b01791.

Hereford, R., 2002, Valley-fill alluviation during the Little Ice Ace (ca. A.D. 1400–1880), Paria River Basin and southern Colorado Plateau, United States: GSA Bulletin, v. 114, no. 12, p. 1550–1563, accessed March 2022 at https://doi.org/10.1130/0016-7606(2002)114%3C1550:VFADTL%3E2.0.CO;2.

Hettinger, R.D., and Kirschbaum, M.A., 2003, Stratigraphy of the Upper Cretaceous Mancos Shale (upper part) and Mesaverde Group in the southern part of the Uinta and Piceance Basins, Utah and Colorado, chap. 12 *of* USGS Uinta-Piceance Assessment Team, Petroleum systems and geologic assessment of oil and gas in the Uinta-Piceance Province, Utah and Colorado: U.S. Geological Survey Digital Data Series DDS–69–B, 21 p., accessed August 9, 2023, at https://doi.org/10.3133/ds69B.

Homan, J.W., 2024, Assessment and characterization of ephemeral stream channel stability and mechanisms affecting erosion in Grand Valley, western Colorado, 2018–21: U.S. Geological Survey Scientific Investigations Report 2023–5145, 33 p., accessed July 9, 2025, at https://doi.org/10.3133/sir20235145.

Kampf, S.K., Gannon, B.M., Wilson, C., Saavedra, F., Miller, M.E., Heldmyer, A., Livneh, B., Nelson, P., and MacDonald, L., 2020, PEMIP—Post-fire erosion model inter-comparison project: Journal of Environmental Management, v. 268, article 110704, accessed May 11, 2026, at https://doi.org/10.1016/j.jenvman.2020.110704

Knighton, D., 1998, Fluvial Forms and Processes—A new perspective [1st edition]: London, U.K., Hodder Education, Hachette Livre U.K., 383 p. [Also available at https://doi.org/10.4324/9780203784662.]

Kulp, T.R., and Pratt, L., 2004, Speciation and weathering of selenium in Upper Cretaceous chalk and shale from South Dakota and Wyoming, U.S.A.: Geochimica et Cosmochimica Acta, v. 68, p. 3687–3701.

Laabs, B., and Munroe, J.S., 2018, The last Pleistocene glaciation in the Uinta Mountains—Updated chronology and connections to Lake Bonneville, *in* 2018 Lake Bonneville Geologic Conference and Short Course, October 3–6, 2018, Proceedings: National Science Foundation, 9 p., accessed April 2025 at https://par.nsf.gov/biblio/10191138-last-pleistocene-glaciation-uinta-mountains-updated-chronology-connections-lake-bonneville.

Lane, E.W., 1954, The importance of fluvial morphology in hydraulic engineering: Bureau of Reclamation Hydraulic Laboratory Report no. 372, 19 p. [Also available at https://semspub.epa.gov/work/01/554355.pdf.]

Laronne, J.B., and Schumm, S.A., 1982, Soluble mineral content in surficial alluvium and associated Mancos Shale: Journal of the American Water Resources Association, v. 18, no. 1, p. 27–35, accessed December 10, 2025, at https://doi.org/10.1111/j.1752-1688.1982.tb04524.x.

Leib, K.J., Linard, J.I., and Williams, C.A., 2012, Statistical relations of salt and selenium loads to geospatial characteristics of corresponding subbasins of the Colorado and Gunnison Rivers in Colorado: U.S. Geological Survey Scientific Investigations Report 2012–5003, 31 p., accessed December 7, 2021, at https://doi.org/10.3133/sir20125003.

Lemly, A.D., 1985, Toxicology of selenium in a freshwater reservoir—Implications for environmental hazard evaluation and safety: Ecotoxicology and Environmental Safety, v. 10, p. 314–338, accessed December 9, 2020, at https://doi.org/10.1016/0147-6513(85)90079-x.]

Lemly, A.D., 2002, Selenium assessment in aquatic ecosystems—A guide for hazard evaluation and water quality criteria: New York, Springer-Verlag, Inc., 161 p. [Also available at https://doi.org/10.1007/978-1-4613-0073-1.]

Leopold, L.B., Emmett, W.W., and Myrick, R., 1966, Channel and hillslope processes in a semiarid area, New Mexico: U.S. Geological Survey Professional Paper 352–G, 57 p. accessed March 2022 at https://doi.org/10.3133/pp352G.

Leopold, L.B., and Maddock, T., 1953, The hydraulic geometry of stream channels and some physiographic implications: U.S. Geological Survey Professional Paper 282–B, p. 39–85. [Also available at https://doi.org/10.3133/pp352G.]

Lew, R., Dobre, M., Srivastava, A., Brooks, E.S., Elliot, W.J., Robichaud, P.R., and Flanagan, D.C., 2022, WEPPcloud—An online watershed-scale hydrologic modeling tool—Part I—Model description: Journal of Hydrology, v. 608, accessed May 11, 2026, at https://doi.org/10.1016/j.jhydrol.2022.127603.

Linard, J.I., 2013, Ranking contributing areas of salt and selenium in the Lower Gunnison River Basin, Colorado, using multiple linear regression models: U.S. Geological Survey Scientific Investigations Report 2013–5075, 45 p., accessed December 7, 2021, at https://doi.org/10.3133/sir20135075.

Lusby, G.C., 1979, Effects of grazing on runoff and sediment yield from desert rangeland at Badger Wash in western Colorado, 1953–73: U.S. Geological Survey Water-Supply Paper 1532–I, 134 p. [Also available at https://doi.org/10.3133/wsp1532I.]

Mackin, J.H., 1948, Concept of the graded river: Bulletin of the Geological Society of America, v. 59, no. 5, p. 463–512. [Also available at https://doi.org/10.1130/0016-7606(1948)59[463:COTGR]2.0.CO;2.]

Mahan, S.A., Donlan, R.A., and Kardos, B., 2015, Luminescence dating of anthropogenic features of the San Luis Valley, Colorado—From stone huts to stone walls: Quaternary International, v. 362, p. 50–62, accessed February 23, 2022, at https://doi.org/10.1016/j.quaint.2014.09.067.

Mahan, S.A., Krolczyk, E.T., and Gidley, R.G., 2026, Geochronologic data for selected subbasins of Stinking Water Gulch, Rio Blanco County, Colorado, 2015–2020: U.S. Geological Survey data release, https://doi.org/10.5066/P9KLLFQT.

Mahan, S.A., Rittenour, T.M., Nelson, M.S., Ataee, N., Brown, N., DeWitt, R., Durcan, J., Evans, M., Feathers, J., Frouin, M., Guerin, G., Heydari, M., Huot, S., Jain, M., Keen-Zebert, A., Li, B., Lopez, G.I., Neudorf, C., Porat, N., Rodrigues, K., Oliveira Sawakuchi, A., Spencer, J.Q.G., and Thomsen, K., 2023, Guide for interpreting and reporting luminescence dating results: GSA Bulletin, v. 135, no. 5–6, p. 1480–1502, accessed March 18, 2025, at https://doi.org/10.1130/B36404.1.

Mast, M.A., Mills, T.J., Paschke, S.S., Keith, G., and Linard, J.I., 2014, Mobilization of selenium from the Mancos Shale and associated soils in the lower Uncompahgre River Basin, Colorado: Applied Geochemistry, v. 48, p. 16–27, accessed June 12, 2023, at https://doi.org/10.1016/j.apgeochem.2014.06.024.

McAuliffe, J.R., Scuderi, L.A., and McFadden, L.D., 2006, Tree-ring record of hillslope erosion and valley floor dynamics—Landscape responses to climate variation during the last 400yr in the Colorado Plateau, northeastern Arizona: Global and Planetary Change, v. 50, no. 3–4, p. 184–201, accessed October 2021 at https://doi.org/10.1016/j.gloplacha.2005.12.003.

McGwire, K.C., Weltz, M.A., Nouwakpo, S., Spaeth, K., Founds, M., and Cadaret, E., 2020, Mapping erosion risk for saline rangelands of the Mancos Shale using the rangeland hydrology erosion model: Land Degradation & Development, v. 31, no. 17, p. 2552–2564, accessed December 15, 2021, at https://doi.org/10.1002/ldr.3620.

Medialdea, A., Thomsen, K.J., Murray, A.S., and Benito, G., 2014, Reliability of equivalent-dose determination and age-models in the OSL dating of historical and modern paleoflood sediments: Quaternary Geochronology, v. 22, p. 11–24, accessed January 19, 2023, at https://doi.org/10.1016/j.quageo.2014.01.004.

Miller, M.P., Buto, S.G., Lambert, P.M., and Rumsey, C.A., 2017, Enhanced and updated spatially referenced statistical assessment of dissolved-solids load sources and transport in streams of the Upper Colorado River Basin: U.S. Geological Survey Scientific Investigations Report 2017–5009, 23 p., accessed December 15, 2021, at https://doi.org/10.3133/sir20175009.

Mills, T.J., Mast, A.M., Thomas, J., and Keith, G., 2016, Controls on selenium distribution and mobilization in an irrigated shallow groundwater system underlain by Mancos Shale (Uncompahgre River Basin, Colorado, U.S.A.: Science of the Total Environment, v. 566–567, p. 1621–1631, accessed January 7, 2026, at https://doi.org/10.1016/j.scitotenv.2016.06.063.

Munyikwa, K., Kinnaird, T.C., and Sanderson, D.C.W., 2020, The potential of portable luminescence readers in geomorphological investigations—A review: Earth Surface Processes and Landforms [early view], accessed December 2, 2020, at https://doi.org/10.1002/esp.4975.

National Centers for Environmental Information, 2023, U.S. climate normals quick access—1991–2020: National Centers for Environmental Information digital data web site, accessed June 12, 2023, at https://www.ncei.noaa.gov/access/us-climate-normals/#dataset=normals-annualseasonal&timeframe=30&station=USC00056832.

National Geodetic Survey, 2017, Online Positioning User Service: National Geodetic Survey web page, accessed May 24, 2017, at https://www.ngs.noaa.gov/OPUS/.

Natural Resources Conservation Service, 2019, Soil health guides for educators—Bulk density/moisture/aeration: U.S. Department of Agriculture Natural Resources Conservation Service web page, 11 p., accessed March 19, 2025, at https://www.nrcs.usda.gov/sites/default/files/2022-10/Soil%20Bulk%20Density%20Moisture%20Aeration.pdf.

Nelson, M.S., Gray, H.J., Johnson, J.A., Rittenour, T.M., Feathers, J.K., and Mahan, S.A., 2015, User guide for luminescence sampling in archaeological and geological contexts: Advances in Archaeological Practice, v. 3, no. 2, p. 166–177, accessed June 1, 2020, at https://doi.org/10.7183/2326-3768.3.2.166.

Ohlendorf, H.M., 1989, Bioaccumulation and effects of selenium in wildlife, *in* Jacobs, L.W., ed., Selenium in agriculture and the environment: American Society of Agronomy and Soil Science Society of America, p. 133–177. [Also available at https://pubs.usgs.gov/publication/5210452.]

Ohlendorf, H.M., Hoffman, D.J., Saiki, M.K., and Aldrich, T.W., 1986, Embryonic mortality and abnormalities of aquatic birds—Apparent impacts by selenium from irrigation drainwater: Science of the Total Environment, v. 52, no. 1–2, p. 49–63, accessed June 26, 2023, at https://doi.org/10.1016/0048-9697(86)90104-X.]

Olley, J., Caitcheon, G., and Murray, A., 1998, The distribution of apparent dose as determined by optically stimulated luminescence in small aliquots of fluvial quartz—Implications for dating young sediments: Quaternary Science Reviews, v. 17, no. 11, p. 1033–1040, accessed January 19, 2023, at https://doi.org/10.1016/S0277-3791(97)00090-5.

Parker, G.G., and Jenne, E.A., 1967, Structural failure of Western highways caused by piping—41st annual meeting of the Highway Research Board, [Washington, D.C.], January 8–12, 1962: U.S. Geological Survey Water Resources Division, p. 57–76.

Pederson, J.L., Anders, M.D., Rittenour, T.M., Sharp, W.D., Gosse, J.C., and Karlstrom, K.E., 2006, Using fill terraces to understand incision rates and evolution of the Colorado River in eastern Grand Canyon, Arizona: Journal of Geophysical Research—Earth Surface, v. 111, no. F2, accessed June 1, 2020, at https://doi.org/10.1029/2004JF000201.

Porat, N., Zilberman, E., Amit, R., and Enzel, Y., 2001, Residual ages of modern sediments in a hyperarid region, Israel: Quaternary Science Reviews, v. 20, no. 5–9, p. 795–798, accessed June 21, 2022, at https://doi.org/10.1016/S0277-3791(00)00021-4.

Poreba, G.J., Snieszko, Z., and Moska, P., 2015, Application of OSL dating and ^{137}Cs measurements to reconstruct the history of water erosion—A case study of a Holocene colluvium in Swierklany, south Poland: Quaternary International, v. 374, p. 189–197, accessed September 2022 at https://doi.org/10.1016/j.quaint.2015.04.004.

Prescott, J.R., and Hutton, J.T., 1994, Cosmic ray contributions to dose rates for luminescence and ESR dating—Large depths and long-term time variations: Radiation Measurements, v. 23., no. 2–3, p. 497–500, accessed July 7, 2020, at https://doi.org/10.1016/1350-4487(94)90086-8.

Presser, T.S., 1994, The Kesterson effect: Environmental Management, v. 18, no. 3, p. 437–454. [Also available at https://doi.org/10.1007/BF02393872.]

Presser, T.S., Sylvester, M.A., and Low, W.H., 1994, Bioaccumulation of selenium from natural geologic sources in western states and its potential consequences: Environmental Management, v. 18, p. 423–436, accessed June 26, 2023, at https://doi.org/10.1007/BF02393871.

Preston, T.M., Day, N.K., Adams, J.D., and Holmquist-Johnson, C.L., 2021, Orthoimagery, digital elevation, digital terrain, final surface, and vegetation classification models for four stream catchments in western Colorado 2016: U.S. Geological Survey data release, https://doi.org/10.5066/P91KRAAD.

R Core Team, 2019a, R—A language and environment for statistical computing (ver. 3.6.1): R Foundation for Statistical Computing, Vienna, Austria, accessed June 2021, at https://www.R-project.org/.

R Core Team, 2019b, stats-package—The R stats package (ver. 3.6.1): R Foundation for Statistical Computing, Vienna, Austria, accessed January 2022 at https://www.R-project.org/.

Reybold, W.U., and TeSelle, G.W., 1989, Soil geographic data bases: Journal of Soil and Water Conservation, v. 44, no. 1, p. 28–29. [Also available at https://www.jswconline.org/content/44/1/28.]

Richards, R.J., 2022, Data from the assessment of sediment-retention ponds near Delta, Colorado, 2019: U.S. Geological Survey data release, accessed January 8, 2026, at https://doi.org/10.5066/P9WZNJL6.

Richards, R.J., Bern, C.R., and Moreno, V., 2023, Assessment of salinity retention or mobilization by sediment-retention ponds near Delta, Colorado, 2019: U.S. Geological Survey Scientific Investigations Report 2023–5071, 21 p., accessed January 8, 2026, at https://doi.org/10.3133/sir20235071.

Richards, R.J., and Moore, J.L., 2015, Characterization of streamflow, salinity, and selenium loading and land-use change in Montrose Arroyo, western Colorado, from 1992 to 2013: U.S. Geological Survey Scientific Investigations Report 2015–5039, 18 p., accessed December 7, 2021, at https://doi.org/10.3133/sir20155039.

Rodnight, H., 2008, How many equivalent dose values are needed to obtain a reproducible distribution?: Ancient TL, v. 26, no. 1, p. 3–10, accessed June 26, 2023, at https://doi.org/10.26034/la.atl.2008.414.]

Rosgen, D.L., 2006, Watershed Assessment of River Stability and Sediment Supply (WARSSS): Fort Collins, Colo., Wildland Hydrology Books, 648 p..

Rydlund, P.H., Jr., and Densmore, B.K., 2012, Methods of practice and guidelines for using survey-grade global navigation satellite systems (GNSS) to establish vertical datum in the United States Geological Survey: U.S. Geological Survey Techniques and Methods, book 11, chap. D1, 102 p. with appendixes. [Also available at https://pubs.usgs.gov/tm/11d1/.]

Schumm, S.A., and Hadley, R.F., 1957, Arroyos and the semiarid cycle of erosion [Wyoming and New Mexico]: American Journal of Science, v. 255, no. 3, p. 161–174, accessed February 2022 at https://doi.org/10.2475/ajs.255.3.161.

Schumm, S.A., Harvey, M.D., and Watson, C.C., 1984, Incised channels—Morphology, dynamics and control: Littleton, Colorado, Water Resources Publications, 200 p.

Schwinning, S., Belnap, J., Bowling, D.R., and Ehleringer, J.R., 2008, Sensitivity of the Colorado Plateau to change—Climate, ecosystems, and society: Ecology and Society, v. 13, no. 2, 20 p., accessed October 2021 at https://www.jstor.org/stable/26268003.

Simon, A., Curini, A., Darby, S.E., and Langendoen, E.J., 2000, Bank and near-bank processes in an incised channel: Journal of Geomorphology, v. 35, p. 193–217, accessed August 30, 2022, at https://doi.org/10.1016/S0169-555X(00)00036-2.

Simon, A., 1989, A model of channel response in disturbed alluvial channels: Earth Surface Processes and Landforms, v. 14, p. 11–26, accessed August 2025 at https://doi.org/10.1002/esp.3290140103.

Simon, A., and Darby, S.E., 1997, Process-form interactions in unstable sand-bed river channels—A numerical modeling approach: Geomorphology, v. 21, no. 2, p. 85–106. [Also available at https://doi.org/10.1016/S0169-555X(97)00043-3.]

Simon, A., and Downs, P.W., 1995, An interdisciplinary approach to evaluation of potential instability in alluvial channels: Geomorphology, v. 12, no. 3, p. 215–32, accessed August 2025 at https://doi.org/10.1016/0169-555X(95)00005-P.

Smedley, R.K., and Skirrow, G.K.A., 2019, Luminescence dating in fluvial settings—Overcoming the challenges of partial bleaching, *in* Herget, J., and Fontana, A., eds., Palaeohydrology: Springer Cham, p. 155–168, accessed November 7, 2022, at https://doi.org/10.1007/978-3-030-23315-0_8.

Steffen, D., Preusser, F., and Schlunegger, F., 2009, OSL quartz age underestimation due to unstable signal components: Quaternary Geochronology, v. 4, no. 5, p. 353–362, accessed February 23, 2022, at https://doi.org/10.1016/j.quageo.2009.05.015.

Summa-Nelson, M.C., and Rittenour, T.M., 2012, Application of OSL dating to middle to late Holocene arroyo sediments in Kanab Creek, southern Utah, U.S.A.: Quaternary Geochronolgy, v. 10, p. 167–174, accessed July 13, 2020, at https://doi.org/10.1016/j.quageo.2012.05.002.

Taggert, J.E., Jr., ed., 2002, Analytical methods for chemical analysis for geologic, and other materials, U.S. Geological Survey (ver. 5.0): U.S. Geological Survey Open-File Report 2002–223, 20 p., accessed February 23, 2022, at https://doi.org/10.3133/ofr02223.

Thomsen, K.J., Murray, A.S., Jain, M., and Botter-Jensen, L., 2008, Laboratory fading rates of various luminescence signals from feldspar-rich sediment extracts: Radiation Measurements, v. 43, no. 9–10, p. 1474–1486, accessed February 23, 2022, at https://doi.org/10.1016/j.radmeas.2008.06.002.

Townsend, K.F., Nelson, M.S., Rittenour, T.M., and Pederson, J.L., 2019, Anatomy and evolution of a dynamic arroyo system, Kanab Creek, southern Utah, U.S.A.: GSA Bulletin, v. 131, no. 11–12, p. 2094–2109, accessed December 2021 at https://doi.org/10.1130/B35195.1.

Trimble, S.W., and Mendel, A.C., 1995, The cow as a geomorphic agent—A critical review: Geomorphology, v. 13, no. 1–4, p. 233–253, accessed June 24, 2022, at https://doi.org/10.1016/0169-555X(95)00028-4.

Tuttle, M.L.W., Fahy, J.W., Elliott, J.G., Grauch, R.I., and Stillings, L.L., 2014, Contaminants from Cretaceous black shale—I. Natural weathering processes controlling contaminant cycling in Mancos Shale, southwestern United States, with an emphasis on salinity and selenium: Applied Geochemistry, v. 46, p. 57–71, accessed June 12, 2023, at https://doi.org/10.1016/j.apgeochem.2013.12.010.

Tuttle, M.L., and Grauch, R.I., 2009, Salinization of the Upper Colorado River—Fingerprinting geologic salt sources: U.S. Geological Survey Scientific Investigations Report 2009–5072, 62 p., accessed June 12, 2023, at https://doi.org/10.3133/sir20095072.

Tweto, O., 1979, Geologic map of Colorado: U.S. Geological Survey, 1:500,000, accessed December 2021 at https://doi.org/10.3133/70211263.

Ullman, S., 1979, The interpretation of structure from motion: Proceedings of the Royal Society of London, Series B, v. 203, no. 1153, p. 405–426, accessed June 9, 2025, at https://doi.org/10.1098/rspb.1979.0006.

U.S. Department of Agriculture, 2001, Soil quality test kit guide: U.S Department of Agriculture web page, 82 p., accessed December 11, 2025, at https://www.nrcs.usda.gov/sites/default/files/2022-10/Soil%20Quality%20Test%20Kit%20Guide.pdf.

U.S. Department of Agriculture, 2004, National elevation dataset 30 meter 1-degree tiles: U.S. Department of Agriculture website, accessed January 24, 2017, at https://datagateway.nrcs.usda.gov/.

U.S. Department of Agriculture Forest Service, 2008, WEPP Road Batch ver. 2008.10.23: U.S. Forest Service web page, accessed January 2017 at https://forest.moscowfsl.wsu.edu/cgi-bin/fswepp/wr/wepproadbat.pl.

U.S. Fish and Wildlife Service, 2009, Final Gunnison River Basin programmatic biological opinion, December 2009: U.S. Fish and Wildlife Service, Ecological Services Lakewood, Colorado, 123 p.

U.S. Geological Survey, 2002, National Assessment of Oil and Gas Project—Uinta-Piceance Province (020) boundary: U.S. Geological Survey data release, accessed December 20, 2021, at https://doi.org/10.5066/P9CECSIT.

U.S. Geological Survey, 2016, EarthExplorer: U.S. Geological Survey website, accessed 2016 at https://earthexplorer.usgs.gov/.

U.S. Geological Survey, 2019, The StreamStats program: U.S. Geological Survey website, accessed July 2025 at https://streamstats.usgs.gov/ss/.

Villarreal, M.L., Pierce, J., Waller, E.K., Chambers, S.N., Duniway, M.C., Fancher, T., Hannon, M.T., Montgomery, G.A., Rexer, K., Simonsen, J., Titolo, A.J., and Uncapher, R., 2023, Geodatabase of oil and gas pads and roads within the Bureau of Land Management's Carlsbad Field Office administrative boundary, New Mexico: U.S. Geological Survey data release, accessed April 3, 2025, at https://doi.org/10.5066/P9GKIPLH.

Wallinga, J., 2002, On the detection of OSL age overestimation using single-aliquot techniques: Geochronometria, v. 21, p. 17–26, accessed August 7, 2023, at https://www.geochronometria.pl/pdf/geo_21/Geo21_02.pdf.

Waters, M.R., and Haynes, C.V., 2001, Late Quaternary arroyo formation and climate change in the American Southwest: Geology, v. 29, no. 5, p. 399–402, accessed March 2022 at https://doi.org/10.1130/0091-7613(2001)029%3C0399:LQAFAC%3E2.0.CO;2.

Williams, C.A., Gidley, R.G., and Stevens, M.R., 2023, Salinity and selenium yield maps derived from geostatistical modeling in the lower Gunnison River Basin, western Colorado, 1992–2013: U.S. Geological Survey Scientific Investigations Report 2023–5013, 37 p., accessed April 2023 at https://doi.org/10.3133/sir20235013.

Williams, H.F.L., Havens, D.L., Banks, K.E., and Wachal, D.J., 2007, Field-based monitoring of sediment runoff from natural gas well sites in Denton County, Texas, U.S.A.: Environmental Geology, v. 55, p. 1463–1471, accessed June 24, 2022, at https://doi.org/10.1007/s00254-007-1096-9.

Wintle, A.G., and Murray, A.S., 2006, A review of quartz optically stimulated luminescence characteristics and their relevance in single-aliquot regeneration dating protocols: Radiation Measurements, v. 41, no. 4, p. 369–391, accessed May 16, 2022, at https://doi.org/10.1016/j.radmeas.2005.11.001.

Womack, W.R., and Schumm, S.A., 1977, Terraces of Douglas Creek, northwestern Colorado—An example of episodic erosion: Geology, v. 5, no. 2, p. 72–76, accessed July 2020 at https://doi.org/10.1130/0091-7613(1977)5%3C72:TODCNC%3E2.0.CO;2.

Zawislanski, P.T., Benson, S.M., TerBerg, R., and Borglin, S.E., 2003, Selenium speciation, solubility, and mobility in land-disposed dredged sediments: Environmental Science and Technology, v. 37, no. 11, p. 2415–2420, accessed November 9, 2022, at https://pubs.acs.org/doi/10.1021/es020977z.

For more information concerning the research in this report, contact
the Director, USGS Colorado Water Science Center
Box 25046, Mail Stop 415
Denver, CO 80225
(303) 236–4882
Or visit the Colorado Water Science Center website at
https://www.usgs.gov/centers/colorado-water-science-center
Publishing support provided by the USGS Science Publishing Network,
Denver, Reston, and Rolla Publishing Service Centers

ISSN 2328-0328 (online)
https://doi.org/10.3133/sir20265048